POLITECNICO DI TORINO

Facoltà di Ingegneria
Corso di Laurea Magistrale in Ingegneria Energetica e Nucleare

Master's thesis

Design and Simulation of the DC Office Lab integrated with photovoltaic systems and storage solutions

Supervisors (in Turin, Italy):
Dr. Andrea Lanzini
Prof. Dr. Pierluigi Leone
Supervisors (in Delft, The Netherlands):
Dr. Carla Robledo
Ir. Jaco Reijerkerk
Prof. Dr. Ad van Wijk

Candidate:
Noemi Barone

13th April 2018
A.A. '17/'18

Acknowledgement

I would like to thank so many people that one page is not enough. In these months I met and I talked to many people who helped me in many ways. First of all, I would like to express gratitude to my thesis advisors in Delft, Prof. Dr. Ad van Wijk, Ir. Jaco Reijerkerk and Dr. Carla Robledo and in Italy Prof. Pierluigi Leone and Dr. Andrea Lanzini. They gave me very helpful tips and suggestions. They were always open to my questions and helped me a lot.

I would also like to acknowledge the TU Delft and The Green Village for the possibility to work on this innovative research. I am so grateful to everyone I met at The Green Village in The Office Lab because each of them guided me patiently throughout the project.

Finally, I want to be very thankful to my parents, my family and my close friends for their continuous support, for believing continuously in my abilities and for their perseverance to be like they are with me. This work and my whole student carrier would not have been possible without anyone of them.

Last but not least, my sincere gratitude and love to those friends I found in the last stage of this long trip, who made me richer than before even when they did not recognize how important were for me.

To all of you, thank you sincerely.

List of figures

Figure 1: The Office Lab at The Green Village. (4) 9

Figure 2: PV system at the Office Lab (Delft), (4). 9

Figure 3: Hydrogen scooter during the first test at The Green Village (10/2017), (4). 9

Figure 5: Low pressure hydrogen canister in the rear side of the hydrogen scooter (4), on the left, and a detail of the metal hydride storage, on the right. 10

Figure 4: One of the two meeting rooms at the Office Lab. The IR panel is the white panel in the middle of the ceiling. The four lights turned on are DC loads as well. (4) 10

Figure 6: Electric scheme of the microgrid in the Office Lab. 15

Figure 7: Monthly average global irradiance in Delft during 2016 and comparison with values in Italy: measured levels in Rotterdam and in Milan (on the left) and clear sky condition (on the right). 16

Figure 8: Simplified map of the Office Lab at The Green Village. (32) 16

Figure 9: Electric scheme of DC grid 18

Figure 10: Compact scheme of the model in Simulink. 18

Figure 12: DC/DC boost converter in the 0.9 kW_p PV system. 20

Figure 11: DC/DC buck converter in the 4.4 kW_p PV system. 20

Figure 13: Flowchart of duty cycle using Perturb and Observe technique in the MPPT block. (34) 21

Figure 14: Inputs and outputs of the controller. 22

Figure 15: On the left, DC electric grid at the Office Lab composed of four lithium-ion batteries. On the right, detail of the lithium-ion battery. 22

Figure 16: Equivalent circuit of rechargeable battery. 23

Figure 17: Three phase inverter DC/AC with IGBT- diode bridge. (36) 23

Figure 18: Compact scheme of the second model in Simulink. 24

Figure 19: I-V and P-V characteristics of PV array in case of 1000 W/m^2 solar irradiance and different cell temperatures (0°C, 25°C and 45 °C). 26

Figure 20: Solar PV inputs in January 2016. The above graph describes the irradiance levels during the month in [W/m^2]; the graph below shows the temperature variation in [°C] during the month. 29

Figure 21: Daily PV panels production in January 2016 (first simulation). 30

Figure 22: Daily energy balance in the high voltage line 350 V_{DC} (January, first simulation). 30

Figure 23: Daily energy balance in the low voltage line 48 V_{DC} (January, first simulation). 31

Figure 24: Daily variation in the State Of Charge of the batteries connected to the low voltage line (January, first simulation). 31

Figure 25: Monthly solar production in [kW] in the microgrid (January, second simulation). The first graph above represents the PV system in the low voltage line; the second one is the PV system in the high voltage line; the last graph is about battery charging and discharging scheme. 32

Figure 26: Battery performance in terms of the state of charge (graph above, in [%]) and current (graph below, in [A]). (January, second simulation). 32

Figure 27: Monthly energy balance in the high voltage line (January, second simulation). 33

Figure 28: Monthly energy balance in the low voltage line (January, second simulation). 33

Figure 29: : Solar PV inputs in February 2016. The above graph describes the monthly irradiance level in [W/m^2]. 34

Figure 30: Monthly solar production in [kW] in both voltage lines, 48V_{DC} in the graph above and 350 V_{DC} below. (February, second simulation). 34

Figure 31: Battery state of charge in [%]. Time in the x-axis is in [s] (February, second simulation). 35

Figure 32: Monthly energy balance in the high voltage line (February, second simulation). 35

Figure 33: Monthly energy balance in the low voltage line (January, second simulation). 35

Figure 34: Solar PV inputs in March 2016. The above graph describes the monthly irradiance level in [W/m^2]; the graph below shows the monthly temperature variation in [°C]. 36

Figure 35: Daily energy balance in the high voltage line 350 V_{DC} (March, first simulation). 36

Figure 36: Daily energy balance in the low voltage line 48 V_{DC} (March, first simulation). 37

Figure 37: Daily variation in the SoC of the batteries connected to the low voltage line (March, first simulation). 37

Figure 38: Monthly solar production in [kW] in both voltage lines: 48V_{DC} in the graph above and 350 V_{DC} below. (March, second simulation). 38

Figure 39: Battery state of charge in [%] (March, second simulation). 39

Figure 40: Energy balance in low voltage line (March 6th – 13th, second simulation). 39

Figure 41: Monthly energy balance in the high voltage line (March, second simulation). 39

Figure 42: Solar PV inputs in April 2016. The above graph describes the monthly irradiance level in [W/m^2]; the graph below shows the monthly temperature variation in [°C]. 40

Figure 43: Monthly energy balance in the high voltage line. (April, second simulation) 40

Figure 44: Daily energy balance in the low voltage line. (April 6th, second simulation). 41

Figure 45: Battery state of charge in [%] (April, second simulation). 41

Figure 46: Monthly irradiance level in May 2016 measured in [W/m^2]. 41

Figure 47: Daily energy balance in the low voltage line 48 V_{DC} (May, first simulation). 42

Figure 48: Daily variation in the SoC of the batteries connected to the low voltage line (May, first simulation). 42

Figure 49: Battery state of charge in [%]. (May, second simulation). 42

Figure 50: Daily energy balance in the low voltage line. (July, second simulation). 43

Figure 51: Daily PV panels production in September 2016 (first simulation). 44

Figure 52: Daily energy balance in the low voltage line 48 V_{DC} (September, first simulation).44

Figure 53: Battery state of charge in [%] (September, second simulation). 44

Figure 54: Energy balance in low voltage line (September 2nd – 10th , second simulation). 45

Figure 55: Monthly energy balance in the high voltage line (October, second simulation). 46

Figure 56: Monthly energy balance in the low voltage line (October, second simulation). 46

Figure 57: Battery state of charge in [%] (October, second simulation). 46

Figure 58: Battery state of charge in [%] (November, second simulation). 47

Figure 59: PEM Electrolyser Cell Polarization curve (plot above) and efficiency curve (plot below), studied in (39). 49

List of tables

Table 1: Nominal parameters in the solar systems. The third column represents the PV system connected to 48 V_{DC}, while the last column is the PV system in the 350 V_{DC}. 19

Table 2: Hydrogen scooter characteristics. (37) (38) 25

Table 3: Some DC load assumptions in both voltage lines in [W]. The low voltage line 48 V_{DC} includes lighting system and USB electrical output; while the high voltage line 350 V_{DC} just the heating system. 27

Table 4: Monthly data collection using the yearly results of the second simulation. 48

Table 5: Monthly hydrogen production and total production hours. 50

Table 6: Monthly amount of fuel cell electric vehicles charged using the excess of energy in the microgrid. 50

Table 7: Comparison between the best daily design and the fixed size of electrolyser. 51

Table of content

Acknowledgement 1

List of figures 2

List of tables 5

Table of content 6

1. Introduction 8

1. 1. Thesis scope 9

1. 2. Research question 10

1. 3. Structure of thesis 11

2. Microgrid research: background and current status 11

2.1. Hydrogen technology: state of art 12

2.2. Vehicle-to-Grid (V2G) connection and hydrogen vehicles: state of art 13

2.3. DC power grids for buildings 13

3. Methodology 14

3.1. Microgrid description and boundaries 14

3.2. Simulation on Matlab/Simulink 17

3.2.1. 1st accurate analysis: Photovoltaic systems and batteries 18

3.2.2. 2nd fast analysis: Photovoltaic systems and batteries 24

3.2.3. Integration of hydrogen technology 24

3.3 Model assumptions and inputs 26

3.3.1. DC loads profile 27

4. Results and discussion 28

4. 1. January 2016 29

4.1.1 First simulation results 29

4.1.2. Results of the second simulation 31

4.2. February 2016 33

4.2.1. Results of the second simulation 34

4.3. March 2016 35

4.3.1. First model results 36

4.3.2. Second simulation results 37

4.4. April 2016 39

4.4.1. Second simulation results 40

4.5. May 2016 41

4.5.1. First simulation results 41

4.5.2. Second simulation results 42

4.6. June 2016 42
4.7. July 2016 43
4.8. August 2016 43
4.9. September 2016 43
4.9.1. First simulation results 43
4.9.2. Second simulation results 44
4.10. October 2016 45
4.10.1. Second simulation results 45
4.11. November 2016 46
4.12. December 2016 47
5. Hydrogen production by water electrolysis 48
6. Conclusion 52
6. 1. Future developments 53
7. References 54

1. Introduction

Nowadays the pursuit of better living conditions as well as the desire for higher living standards are increasing the energy demands in a context of rapid economic growth and dense urban populations.
The households and transport sectors account the biggest final energy consumption after the manufacturing energy sector on a global scale. In more detail, in the European Union (EU), building and transportation sectors have accounted for around 60% of the final energy consumption. (1)
The near future prospect accounts the significant reduction of CO_2 emissions. More specifically, the EU 2050 roadmap defines a reduction of around 90% energy savings in building energy sector and 60% in transportation, compared to the 1990 emissions levels. (2)
In this view, the development is moving through innovative changes in the energy sector in order to provide environmentally friendly energy and re-use of waste energy.
The main goal is to make dispatchable the non-dispatchable energy supply by renewable sources. The most used renewable energy sources are wind turbines and photovoltaic panels. The biggest problem due to the integration of renewable power generation is their intermittency. The main electric grid could have problems in stability, reliability and power quality. A possible solution is the integration of energy storages in the system. Indeed, solar systems are usually combined with batteries, although the most powerful storage is hydrogen.
Thus, the new hybrid main grid has to increase efficiency, safety and involve network management, without any shortage or voltage drop due to the unpredictable and oscillating renewable energy production. Above all, the utility grid has to be flexible. According to the International Energy Agency, the existing infrastructure systems will change to achieve the latter purpose. Moreover, new buildings starting from 2021 have to be nearly zero energy buildings according to the EU Directive 2010/31/EU. (3)
Whereas the development of renewable technologies is combined with storage solutions, the energy consumption will be reduced and, consequently, the Greenhouse Gas (GHG) emissions will decrease.
The future electric grid, called also the smart grid, will monitor and manage in real time the production, distribution and consumption of electric energy. The concept is to produce and re-use energy in the smartest and cleanest way.
According to that, more distributed energy sources are installed in the grid. The result is an increase in the self-consumption, the reduction of GHG emissions and an improvement in the two-ways flow of electricity and information. For example, electric vehicles are often connected in the microgrid in the Vehicle to Grid (V2G) mode in order to provide or demand energy to loads. The amount of variable renewable sources and electric vehicles, installed in the microgrid, is going to bring us to a widespread smart grid where each consumer has the possibility to buy, use or sell the energy of these clean technologies strategically.
In this world, the Car as Power Plant (CaPP) project has born some years ago. More in detail, the project implements hydrogen technologies in the car to power loads when the car is parked.
During the past months, the project has integrated light-weight Fuel Cell Electric Vehicles (FCEV) in the mini-CaPP work. The vehicle works with small variations; it can reduce the peak consumption but it cannot be the main storage solution in the microgrid because of its capacity. It could the best solution in no power situations like camping or emergency

purposes such as off-road situations.
The concept of microgrid integrated with photovoltaic panels, batteries and hydrogen scooters is studied in these pages. The system is working for real since February 2018 in the Office Lab at The Green Village in the TU Delft University, see Figure 1.

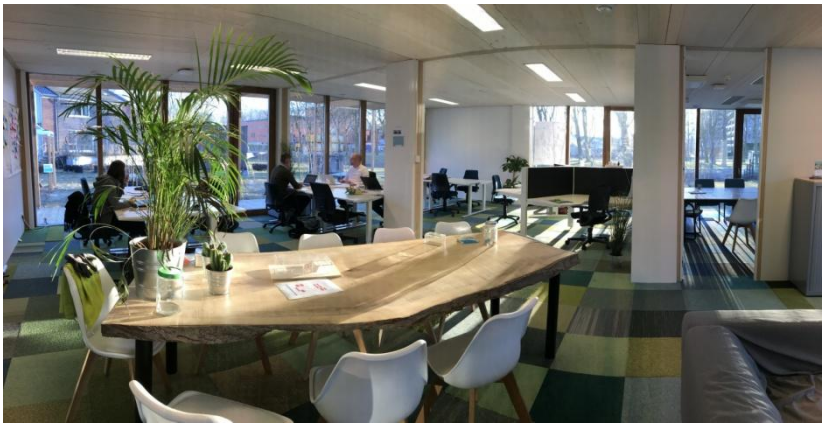

Figure 1: The Office Lab at The Green Village. (4)

1. 1. Thesis scope

In this paper, a case study is used to model and to simulate the electrical scheme of AC/DC connection within an office building. The Office Lab is located in Delft, at The Green Village in the university campus of TU Delft. The microgrid is composed of two photovoltaic systems on the roof (Figure 2), batteries, DC and AC loads.
The model is built on MATLAB/Simulink.
Furthermore, the connection of Fuel Cell Electric Vehicles (FCEVs) in the microgrid is analysed in order to assess if it is feasible to produce hydrogen using the excess of energy from the renewable sources. In this way, the excess of production is not sent to the grid as exported energy and it is used in a more efficient way. In more detail, the case study implements FCEVs as hydrogen scooters. The first scooter has been tested on 30th November 2017 at TU Delft in partnership with Asia Pacific Fuel Cell Technologies (APFCT), see Figure 3.
The integration of light-weight fuel cell electric vehicles in the energy system is developed as a new concept within the Car as Power Plant Project, namely the *mini-CaPP*. The choice of hydrogen scooters instead of cars is mainly because they require a small amount of hydrogen in their tank and lower pressure compared to FC electric cars; the detailed description is in Paragraph 3.2.3. Integration of hydrogen technology in the next pages.

Figure 2: PV system at the Office Lab (Delft), (4).

Figure 3: Hydrogen scooter during the first test at The Green Village (10/2017), (4).

The aim of the study is to show and to compare the advantages of using renewable sources combined with V2G technology. When parked, the vehicle is used to feed electricity to the office or directly power loads in the connection as Vehicle-to-Load and Vehicle-to-Home; the choice depends by production and consumption in a particular moment of the day; generally speaking, the connection is called Vehicle-to-X because the vehicle connections could change (to load, home or grid).

The new DC electrical layout in the office building at The Green Village is connected and is working since February 2018 in two meeting rooms. Whereas part of the office starts to work in DC scheme, the Simulink system provides useful information about the annual interaction between DC office, photovoltaic systems and the utility grid.

Figure 4: One of the two meeting rooms at the Office Lab. The IR panel is the white panel in the middle of the ceiling. The four lights turned on are DC loads as well. (4)

The two companies, *Rexel* and *Engie*, started the research in the DC Office Lab at The Green Village to test the AC/DC mix. First, the combination of AC and DC together will allow energy losses reduction. The ultimate goal will be the fully DC electric setup in The Office Lab. At this stage, only the two meeting rooms in the Office Lab are testing the DC grid; the electric equipment of the room is composed of DC loads as DC plugs, LED lights and IR panels, see Figure 4.

In the near future, the same small-scale project could be carried out in other and bigger buildings in order to evaluate the effectiveness of analogous changes. This paper contributes to the existing research by exploring storage solutions like batteries and hydrogen connected to the PV systems and to the electric grid. Accordingly, the integration of renewable energy source and, moreover, storage devices will contribute to microgrid stability in the office and it will decrease or avoid grid dependence.

1. 2. Research question

The main research question is: *What are the main technologic improvements due to the integration of storage technologies in DC office?*

In order to give an answer to this question, the analysis is focused on the yearly energy balance in the Office Lab. The idea is to measure the annual interaction between the building and the grid with batteries; then in the second part of the study, the amount of hydrogen that could be produced is calculated taking into account the annual excess of solar energy.

Figure 5: Low pressure hydrogen canister in the rear side of the hydrogen scooter (4), on the left, and a detail of the metal hydride storage, on the right.

Consequently, the work calculates the amount of hydrogen and the number of canisters (Figure 5) that could be filled in order to avoid the exported energy to the utility grid. In few words, the energy will be delivered to loads in the office by sources as sun, batteries, hydrogen or the main grid.

1. 3. Structure of thesis

Chapter 2 describes the theoretical background of the thesis topic and its state of art.
In Chapter 3, the model is described using the main components presented in Simulink environment. To answer the research question, the study is divided into two steps: the first system reflects how the actual office works at The Green Village; the second system implements the PEM fuel cell and electrolyser. Chapter 3 gives information also about the input values, load profile and all the assumptions.
Chapter 4 collect the output data from the simulation and discuss the results taking into account the possibility to produce hydrogen. Indeed, hydrogen production and the related assumptions are well described in Chapter 5. Final conclusions are presented in Chapter 6.

2. Microgrid research: background and current status

In the near future, the utility grid should deal with the intermittency of renewable energy sources and the availability of the energy storage system which are the basic components of a local, low-voltage microgrid. According to *Oxford dictionaries* a microgrid is: "A small network of electricity users with a local source of supply" which is called also distributed energy source and it is usually a renewable energy source. This network is "attached to a centralized national grid and able to function also independently" (5). This means that power could enter the grid from dispersed individual residences, and especially if this fraction becomes large enough the power flow through substations would be reversed. Thus, the traditional electric grid needs to be improved with control and communication technologies in order to be updated about power flux and in order to respond to the energy variation in the smartest way possible. (6) (7)
As proof, one of the priorities in the EPRI (Electric Power Research Institute) Roadmap for the 21st century is the development of dynamic two-way communication devices with the purpose of including distributed generation, renewable energy, as well as vehicle-to-grid (V2G) connections. (7) (8)
Smart grids take the advantages of integration of various microgrid systems. In this view, the fluctuation and intermittency of the renewable energy sources need to be overcome using also adequate and acceptable energy policies. Indeed, for example, peak load management is an essential aspect of smart grids. The peak in energy production is shifted in phase with the peak of load consumptions in order to collect daily or seasonally energy savings. With the same aim, some years ago, Europe policies stimulated the self-consumption of locally generated energy, as described in (9). Mainly, in the near future the self-consumption of renewable energy will increase and the grid stability and its functioning have to be ensured.
Further transformations in the layout of the grid include alternative solutions to the current electrical system like, not only distributed energy sources, but also the integration of electric vehicles as small back-up power systems. Some important benefits due to the vehicle-to-grid connection in smart grids are that electric cars are used both as flexible demand sources and

as storage options. (7) (10) (11) (12) (13) Following this idea, not only the utility grid is used less in the microgrid, but also the excess energy from renewable resources is stored in the electric vehicles when they are available.
In the literature, many projects have been focused on using electric vehicles directly linked to a building via the so-called Vehicle to Building (V2B) interactions. Paper (14) shows the benefits of smart charging electric vehicles with photovoltaic power; it leads obviously to an increase of self-consumption of renewable energy on-site.
The spread of electric vehicles technology can impact the grid positively and negatively. The demand cycle for charging could be added unfavourably to the existing peak demand or the charging configuration could be performed interactively with signals from utilities in order to minimise the impact on peak demand. (14) A smart meter could manage the home energy requirement according to reduce peak loads and to enhance the grid stability and reliability, as well described in (15).
Briefly, the utility grid should improve and should allow two-way flow of electricity considering that the number of electric vehicles will grow considerably in the near future.

2.1. Hydrogen technology: state of art

The future energy network will be different compared to the current one. According to (16), the future is described in the paper as the period of 'economic of power'. Future prospects will be characterized by an improvement in the energy performance of new buildings, an increase in the electrical demand due to a big amount of electrical appliances and a bigger on-site generation of renewable electricity. The result of these changes is an urgent demand for advanced and efficient energy storage solutions. There are a lot of possibilities to store the energy in forms of chemical energy using batteries or hydrogen, thermal energy with heat storages, mechanical energy, gravitational, etc.
The future energy network should consider the electrical, fuel and thermal grid as a whole system in which there is a high level of interactions between each part, as (17) suggests.
The integration of the renewable energy sources could be enhanced by the production of hydrogen through electrolysers. The hydrogen cycle is inefficient if one looks only at the electrical side. However, the production chain includes heat and transportation generation as a fuel, too. Thus, the future energy network results in more stability, flexibility and higher energy efficiency. (17)
Hydrogen technology represents the best solution in a stand-alone energy system. In (18), a hybrid solar hydrogen energy system is studied to supply electricity to a mobile house in Mexico.
Instead, Cao *et al.* focused on the connection between electric vehicles and buildings in order to meet the target of zero energy buildings as the European Union 2050 roadmap has settled in Directive 2010/31/EU. Their hybrid systems in Finland and Germany are able to match the optimal combination of PV system, wind turbines and hydrogen storage with the vehicle in around 81-85% of autonomous standalone status (19).
An analogous project is built on Matlab/Simulink in (20), in which the mathematical model designs a grid disconnected passive house with PV modules, battery and hydrogen technology in one random day.

2.2. Vehicle-to-Grid (V2G) connection and hydrogen vehicles: state of art

Since in the near future, the number of electric vehicles will grow considerably, they represent appreciable opportunities as dispatchable energy sources because batteries can be considered as potential energy storage systems and connected to the grid, while parked. Indeed, the collected energy in the vehicle is available to be used for both transportation and building purposes thanks to the V2G connection. Essentially, the idea is to use electric cars in the most efficient way; for example in (21), a bigger view of the same goal is the simulation of a parking lot which could be used as a power provider to the grid. As a result, cars work as controllable power generation units. The goal is to reach a high level of aggregation of vehicles and consequently, a high energy production rate. Thus, a flexible power plant is built and the most powerful exploitation of energy from the electric car is performed.

The requirement of zero energy buildings by EU could be easily satisfied by integrating hydrogen vehicles. Thus, the hydrogen refuelling station is conveniently accessible and the electrolysis of hydrogen can work because of surplus in energy production on-site. The result is the highest matching capability between generation, storage and end-users. Hydrogen system works in two configurations: as a sink to avoid exported energy and as a power backup system when it is necessary. As a result, this configuration with hydrogen technology is also a zero emission fuel if it is connected directly to renewable sources to produce hydrogen via electrolysis, as described in (22).

It should be noticed that as *Guille C. et all* studied in (23), the hydrogen tank inside the electric vehicles is too small to make a significant impact on the grid by itself, also according to the idea in (21). Indeed, the project described in this pages takes into account more than one vehicle as a result of more workers who could travel to their workplace with the own fuel cell electric vehicles.

The first concept comes from the project 'Our Car as our Power Plant' (CaPP) by Ad van Wijk and Leendert Verhoef (24) in which the main aim is to produce electricity from hydrogen when the fuel cell electric vehicle is not used for transportation and it is parked. Indeed a common car is usually used just 5% of the time for transportation; thus, people could take the advantage of energy production when the car is available. (24)

2.3. DC power grids for buildings

The actual Alternate Current (AC) network is inefficient; energy is lost due to use of rectifiers and inverters that work with conversions from DC/AC and then again AC/DC. Besides that, a lot of material like copper is needed for each conversion. The use of Direct Current (DC) in buildings helps to increase the energy efficiency of distribution systems and applications while also reducing the amount of material needed. (25)

The changes described could be done with insignificantly small investment to the consumer and the new system is easily implemented due to many reasons. First, a DC bus already exists in buildings where a photovoltaic system and/or battery are installed. Moreover, many office applications like laptops, screens, printers and also lights and heating system operate with DC voltages. The aim is to save energy because of direct use of DC electricity sources like photovoltaic solar systems; in this view, each application needs just a DC/DC converter. The losses are reduced not only because AC/DC rectifiers are avoided but also because the power cables work better with DC voltage levels than AC ones. Indeed as (26) proved, the power consumption in the lighting system is reduced by 50% in a DC grid test bed compared to the traditional AC grid using LED lights installation instead of fluorescent luminaries. The

installation of LED in 380 V_{DC}, as in (26), implies that higher voltages are transferring the same power as AC voltage lines, so smaller currents are involved and losses are reduced. Higher distribution efficiency results in higher currents flowing in the existing wires; conversely, cables and wires could be thinner that means material savings.
The DC configuration is studied in street lighting too, in (27). Three projects are realized and monitored by The Hague University of Applied Sciences, even if the lack of proper standards suitable for DC grids is the biggest obstacle. As (27) states, the Netherlands guideline NEN1010 describes general instruction about the installation and usage of electricity in buildings in AC and DC grids; but DC electric setup is not clearly explained. The main challenges are the standardization and electronic safety of DC grids, not only in Holland; there are no international standards about the implementation of a DC electric infrastructure.

3. Methodology

The structure and components of the model are described in this chapter.
The project is based on the electrical scheme of the Office Lab at The Green Village, more specifically the focus is on its change from totally AC grid to DC/AC grid. The model works in Matlab/Simulink environment.
The main aim of the research is to study the feasibility of the system and its potential advantages compared to the traditional AC electric scheme. In order to reach this goal, the work is carried out in the following way: the measurement of the energy consumption in the Office Lab are studied as the energy balance between the main grid combined to solar system and storage solutions. The model analyses the possibility to increase the self-consumption of solar energy by using batteries and smart charging of fuel cell electric vehicles. In this way, the photovoltaic power will be consumed within the microgrid as much as possible.
The paper calculates also the charge of the canisters in the electric vehicles with the aim of avoiding completely energy sent to the main grid; although it does not study other variables that might be of interest, like the availability of the vehicles by hour, the unpredictable state of charge in the vehicles in the morning or even the possibility to charge vehicles using the utility grid when it is more convenient. These variables could be studied in a more appropriated project about control and management of such a system.

3.1. Microgrid description and boundaries

Figure 6 presents an overview of the microgrid analysed in this paper. The system is divided into three main groups, highlighted by red rectangular boxes: generators on left, loads on the right and in the middle box their connection allowed using converters.
The power is delivered by two photovoltaic systems and if needed, by the utility grid. Thus, the two photovoltaic systems and the grid are classified as generation sources. In more detail, the model integrates two separated photovoltaic systems, each one feeds a different DC voltage line, 48 V_{DC} or 350 V_{DC}. The bigger PV system could reach the maximum power generation of 4.4 kW; its energy production is delivered to DC loads and batteries going through the low voltage line, 48 V_{DC}. The smaller PV system could produce 0.9 kW during the best weather condition with the highest solar irradiance level of 1000 W/m^2; it is connected to DC loads through the high voltage line, 350 V_{DC}.
The utility grid acts in two way: as a sink when an excess of production from renewable source occurs and as a generation source when the solar system cannot provide enough energy to loads.

There are two DC/AC inverters to connect the two DC voltage lines and the main AC grid.
The office is arranged with plugs in AC and DC outputs, depending on the electric devices that could be connected, like monitors, printers, laptops, phone chargers, lights and electric heating system.

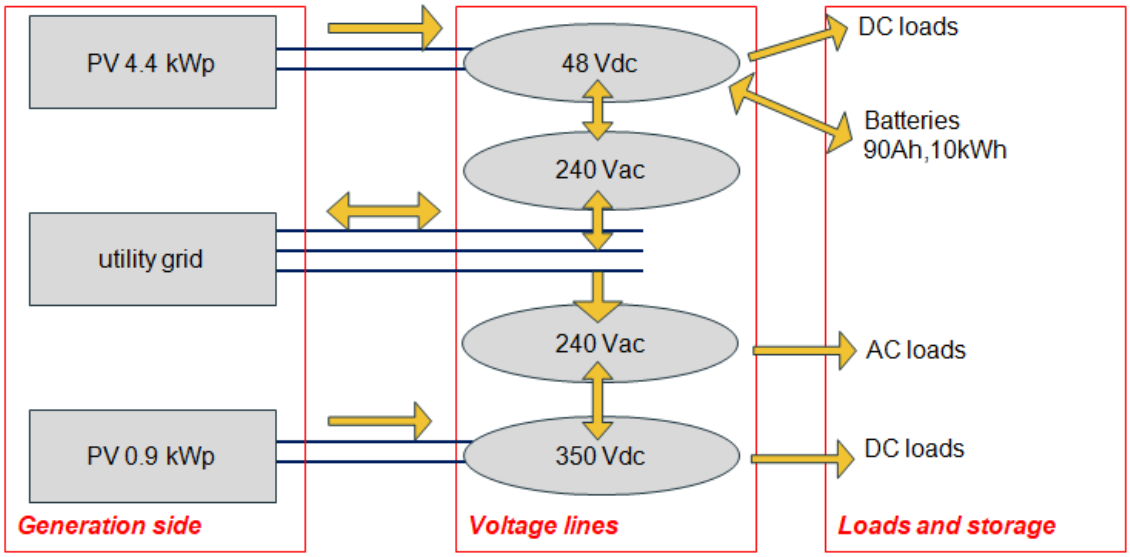

Figure 6: Electric scheme of the microgrid in the Office Lab.

The solar energy is used to feed the loads in the office and/or to charge the batteries. In case of power shortage, electricity is drawn from the main grid. In case of excess of solar energy, electricity is fed back into the main grid.
It is worth to say that the PV system works approximately in the same work hours as the office. Thus, the positive effect is that the electric production and demand are in phase. At the same time, an opposite aspect should be highlighted. The highest electric consumption due to IR panels occurs during the winter season when the solar irradiance presents the lowest values in the year. The lighting system is used more during winter as well because of low availability of sunlight and less solar hours in a day than in the summer period. Thus, the batteries are discharged more in winter than in summer.
One of the biggest problems is presented by weather conditions; indeed global irradiance in The Netherlands is extremely low if compared to the same levels at the same place in clear sky conditions (28). Figure 7 shows the comparison per month. The real measured values (29) of irradiance are three or four times lower than the expected ones on a sunny day. Thus, the photovoltaic power is very unpredictable and unstable in The Netherlands and storages are necessary to keep it constant as much as possible.
In comparison to the Dutch weather condition, the average monthly value in February in Milan (Italy) is shown with the red line and cross signs in order to appreciate the difference and the limited solar power available in North Europe (30). The maximum availability of solar power in The Netherlands during summer is lower than the same value in Italy, in February. Obviously, during summer, the solar production will be even higher in Italy.
Nowadays, the building at The Green Village is working connected to the main grid mostly, equipped with AC loads. Only two meeting rooms are testing DC grid. The idea is to supply entirely the Office Lab with DC equipment in the near future. As shown in Figure 8, the meeting rooms cover around one-sixth of the total area of the office (250 m^2). Hence, the highest electric and heat consumption is accounted for the open space in the main hall. Whereas these rooms are used few times in a day, it means that the overall consumption will

change by a little amount in the new DC/AC office configuration; while the biggest improvement will be provided by full conversion in DC loads.

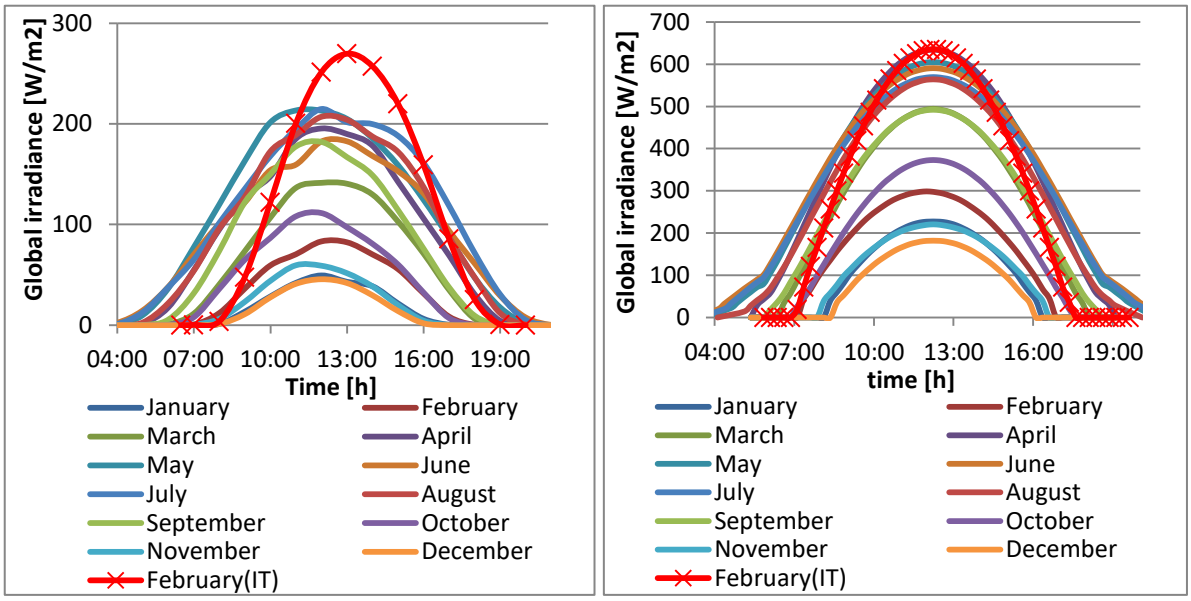

Figure 7: Monthly average global irradiance in Delft during 2016 and comparison with values in Italy: measured levels in Rotterdam and in Milan (on the left) and clear sky condition (on the right).

The choice of using two DC lines is because The Green Village team wants to study and to understand which one is more efficient.

In the literature, many articles study the advantages of high DC voltage lines taking into account losses, costs and savings (26) (27) (30). Nonetheless, the two main reasons for selecting low DC voltages are: the use of many applications in office buildings which work with low DC voltage lines, and the most common voltage connection between photovoltaic systems and batteries.

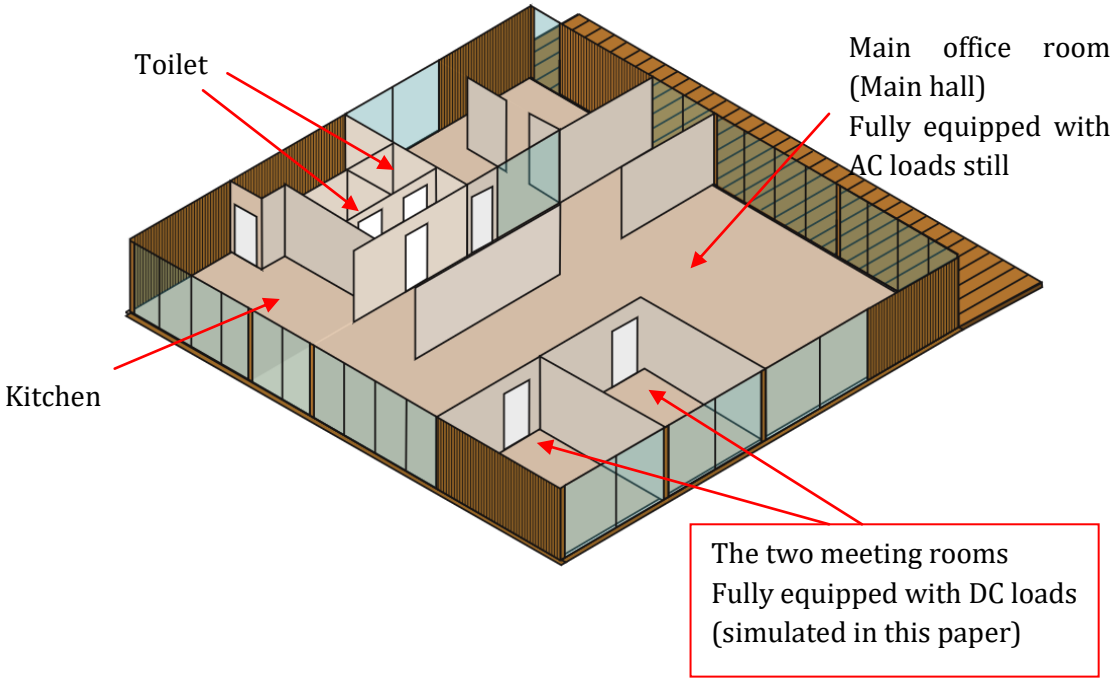

Figure 8: Simplified map of the Office Lab at The Green Village. (32)

3.2. Simulation on Matlab/Simulink

The model of the two meeting rooms is built in Matlab/Simulink environment.
The simulation is split into two parts that are studied sequentially: the first study is about the system composed by photovoltaic modules, batteries, DC loads and utility grid connection; then the model is upgraded with light-weight fuel cell electric scooters that are connected directly to the part of the grid working in 48 V_{DC}.
In the simulation, the electric loads are modelled as resistive loads in both the DC voltage lines. The inputs of the model in terms of solar irradiance and temperature are taken from Royal Netherlands Meteorological Institute during year 2016 (31), even if the DC Office Lab was not installed yet at that time at The Green Village. The choice about the year 2016 was made considering the closest year with full data from January to December. The load profile data are supposed starting from the real AC consumption available in (32) and the consumptions are measured in [Wh] during the simulated days.
It is worth mentioning the rule used in this paper about the sign of electric power in panels, batteries, loads and grid. The power is defined as positive if it is flowing out of source components like PV panels and batteries (in discharging mode), while the positive power flow in load components is power consumed. In this way, the 'generator-load convention' is used: voltage and current variables are defined according to the active sign convention in source components, thus the current is flowing from the negative to the positive terminal of the device; the same variables are defined according to the normal passive sign convention in loads and batteries (in charging mode), thus current is entering the positive terminal. (33)
The utility grid works in passive sign convention as a sink: the power flow in excess sent to the grid is positive, conversely the power delivery by the grid is defined as a negative value.
The matching of the power profiles has been realized on a minute temporal resolution data. The Simscape Power System runs using 5e-6 s sample time due to the presence of controller components and converters from DC to AC voltage. The simulation is a copy of the actual electric scheme used in the building; it works very accurately and slowly because of system configuration. Given the limited time for a Master's thesis, this accurate model simulates just one day per each month. The simulated day is built by an hourly average of the irradiance level during each day in the month, in order to take into account that the weather conditions change a lot during the entire month. In this way, the effect of cloudy days is included in the average day of the simulation.
Another model is built to analyse the fluctuation of batteries during all year 2016. It works faster than the main one because it calculates only the energy balances between production and consumption without modelling each conversion step. Thus, the main difference between the first accurate model and this second fast simulation is the increase in speed due to step size. The first model works with fixed step solver and the maximum step size is fixed by electric devices to 5e-6 s, while the second one uses variable-step solver whose step size is chosen at each time step according to the results of the previous one.
The connection between the office and the utility grid is not modelled in the second system as in the first system; indeed the first accurate system is more complex and exact. The energy balance between grid and the office is not directly measured in the second model; it is derived as a difference. When battery and photovoltaic system cannot provide enough energy to loads, the rest of the load consumption is fed by the utility grid.

3.2.1. 1st accurate analysis: Photovoltaic systems and batteries

The simulation model is a very good representation of the DC electric system at the Office Lab which started working between the end of January and beginning of February 2018. On Simulink, the system reflects the decision taken about PV panels, batteries and loads by a team composed of *Victron*, *Engie*, *Rexel, The Green Village* and TU Delft experts. The electric scheme is resumed in the following Figure 9.

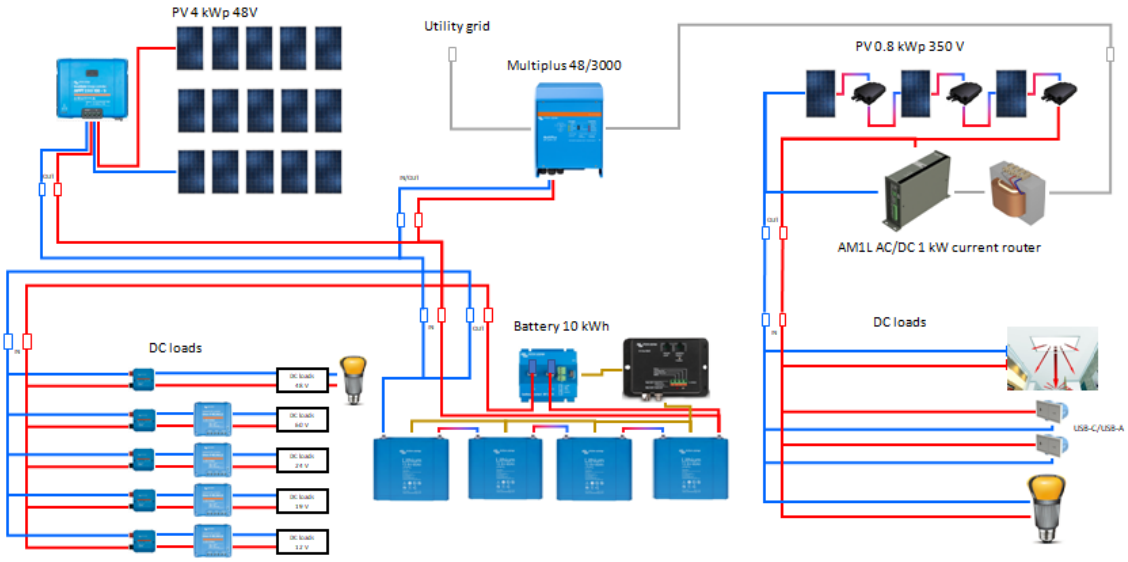

Figure 9: Electric scheme of DC grid

Starting from Figure 9, the corresponding model on Simulink is presented in the compact scheme in Figure 10. The five main components of the microgrid are photovoltaic installations, energy management system, loads, batteries and connection to the main grid. Batteries and PV panels are described using existing modules on Simulink, in which some input parameters are required like the nominal power and voltage, the initial state of charge in batteries and preset modules in PV systems. The other blocks in Figure 10 are built during the analysis, like DC/DC converter, DC/AC inverter, LC filter and the utility grid. The latter components are studied and structured with the help of some papers.

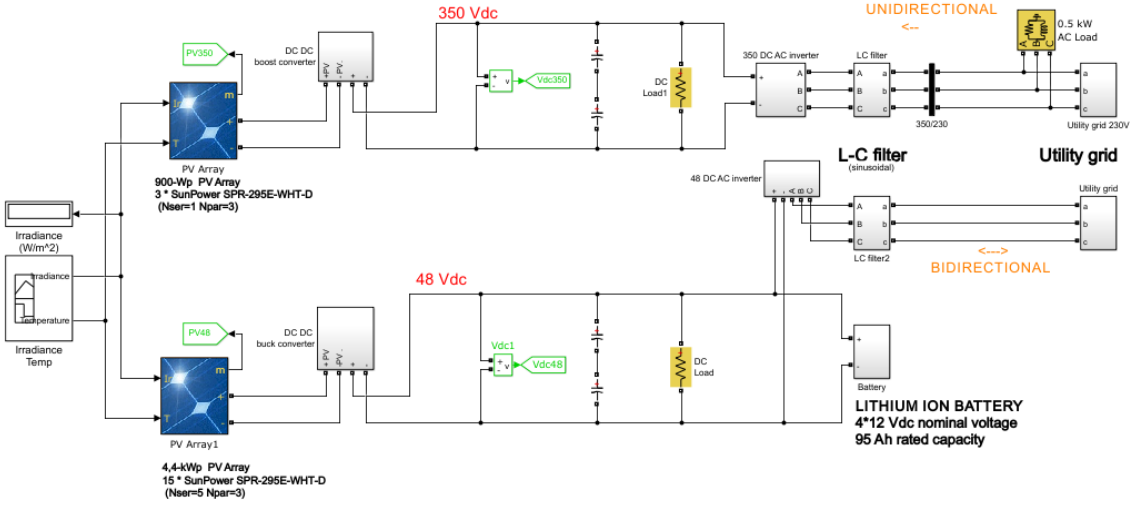

Figure 10: Compact scheme of the model in Simulink.

The first block on the left, called 'Irradiance Temp', gives inputs to panels in terms of irradiance level in $\left[\frac{W}{m^2}\right]$ and cell temperature [°C]. The panels are chosen from datasheet, preset from the National Renewable Energy Laboratory System Advisor Model and according to the capacity already installed at the office. The choice is SunPower SPR-295E-WHT-D, that means that the maximum power of a module is 295 W; 54.2 V and 5.45 A are respectively voltage and current at maximum power point; 63.3 V and 5.83 A are open circuit voltage and short circuit current in that order, as in Table 1.
The diode I-V characteristics for a single module and for a given cell temperature are defined by Equation (1) and Equation (2), in which k is the Boltzman constant equal to 1.38e-23 $\frac{J}{K}$, q is the electron charge 1.6022e-19 C, T is the cell temperature in [K], n_I is the diode ideality factor close to 1, I_0 is the diode saturation current in [A], I_d is the diode current in [A] and N_{cell} is the number of cells connected in series in a module.

Table 1: Nominal parameters in the solar systems. The third column represents the PV system connected to 48 V_{DC}, while the last column is the PV system in the 350 V_{DC}.

	1 module SunPower SPR-295E-WHT-U	**Array 3x5** SunPower SPR-295E-WHT-U	**Array 3x1** SunPower SPR-295E-WHT-U
Maximum Power [W]	295.39	4430.85	886.17
Open Circuit Voltage [V]	63.3	316.5	63.3
Voltage at MPP [V]	54.2	271.0	54.2
Short-circuit current [A]	5.83	17.49	17.49
Current at MPP [A]	5.45	16.35	16.35

PV panels are on the left part of the scheme in Figure 10. The two blocks reflect the real PV parameters. The first block in the upper part is composed of three parallel strings with only one module; while the second block (the bottom of Figure 10) is composed of three parallel strings and five modules connected in series per each string; the result is nearly 0.9 kW_p in the first PV system and 4.4 kW_p in the second one.
The outputs are collected in terms of photovoltaic voltage, current and the resulting power.

$$V = \frac{kT}{q} n_I N_{cell} \quad (1)$$

$$I_d = I_0 \left(\exp\left(\frac{V_d}{V_T}\right) - 1 \right) \quad (2)$$

After PV panels, the model needs a DC/DC boost converter in order to increase the voltage in the high voltage line to 350 V_{DC} and a DC/DC buck converter to decrease the voltage coming from the second solar system to 48 V_{DC}. The detailed models of both DC/DC converters are illustrated in Figure 11 and Figure 12.

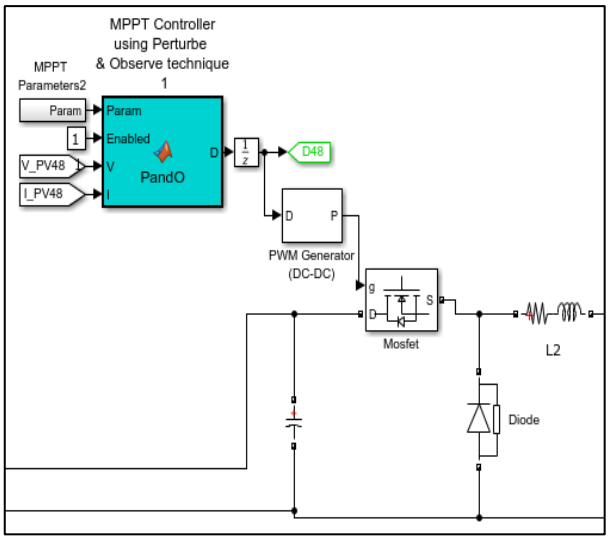

Figure 11: DC/DC buck converter in the 4.4 kW_p PV system.

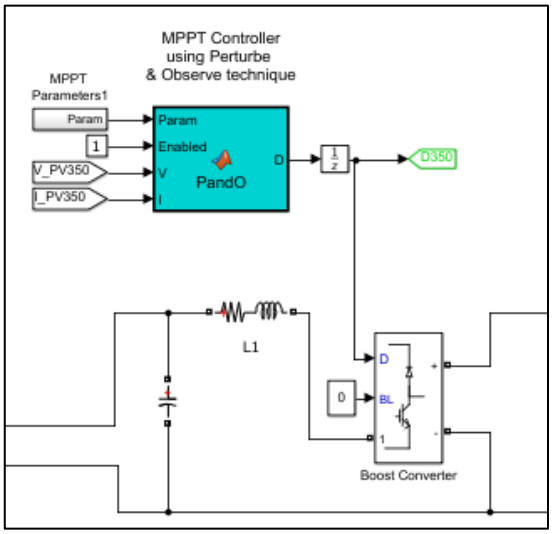

Figure 12: DC/DC boost converter in the 0.9 kW_p PV system.

The converters inputs are PV voltage and current in order to set parameters like the initial value of duty cycle, its upper and lower limit confined between 0 and 1 and its increment value.

The converters are driven by a Maximum Power Point Tracker (MPPT) controller using Perturb and Observe (P&O) technique, integrated in the cyan boxes. The MPPT strategy is based on an iterative method written in a Matlab code: at each time step, the PV power is calculated and consequently it is compared to the same value at the previous step. Then, the voltage value is incremented or decremented in order to reach the maximum power point at each time. The procedure is presented in the flowchart in Figure 13.

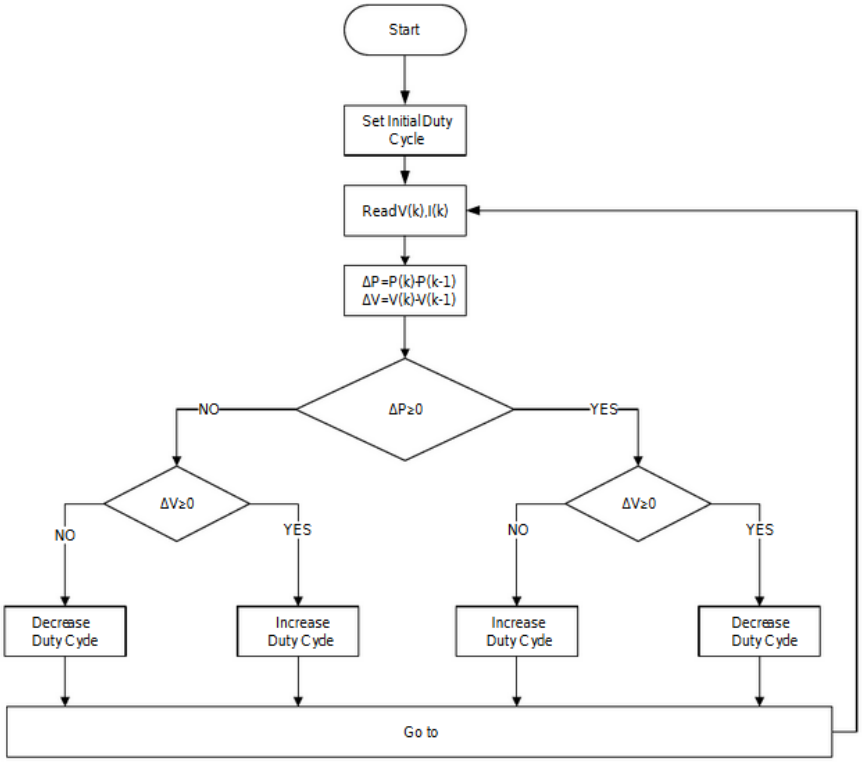

Figure 13: Flowchart of duty cycle using Perturb and Observe technique in the MPPT block. (34)

Boost converter sets the duty cycle (D) using the equation (3) in order to deliver the maximum available power, in which V_{input} is the output voltage of the photovoltaic system, V_{output} is the nominal output voltage of boost converter, 350 V_{DC} in this case study.

$$D = 1 - \frac{V_{input}}{V_{output}} \quad (3)$$

$$D = \frac{V_{output}}{V_{input}} \quad (4)$$

Conversely, buck convert sets the duty cycle using the expression (4), in which where V_{input} is the output voltage of the photovoltaic system and V_{output} is the nominal output voltage of buck converter, 48 V_{DC}.

From these equations, it is easy to understand that since the duty cycle is a number always positive and less than 1, the buck converter can only result in an output voltage smaller than the input voltage ($V_{input} > V_{output}$), while the boost converter can only produce an output voltage bigger than the input voltage ($V_{input} < V_{output}$). (35)

When the duty cycle is calculated, it is converted to digital pulses in order to be sent to the transistor.

Subsequently, the electric system is split between DC loads, battery in the 48 V_{DC} line and DC/AC conversions. For this reason, a control unit is needed to balance supply and demand. The controller changes the parameters in the switches in order to connect and disconnect batteries or utility grid. The controller unit works in a Matlab function file called 'batt_control'. The function takes as inputs at each time step the state of charge in the battery (SOC) combined with its upper and lower limit; in addition, the power from PV system is compared to the load profile consumption.

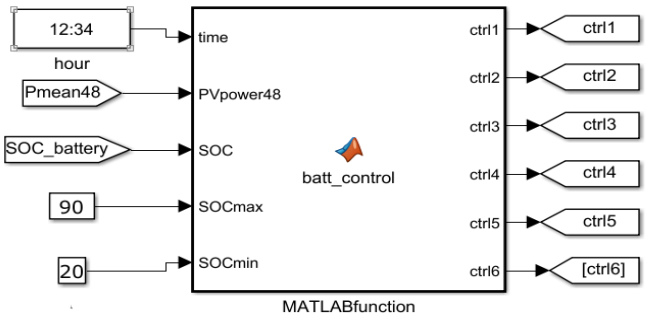

Figure 14: Inputs and outputs of the controller.

The switch control, shown in Figure 14, results in six operation condition described in the following way:

- Switches named *ctrl1, ctrl6, ctrl4, ctrl5* manage DC loads in 48 V_{DC} and 350 V_{DC};
- Control gate *ctrl2* connects PV system and batteries in the 48 V_{DC} line;
- Switch *ctrl3* is the link between the low voltage DC line and AC grid.

The controller connects or disconnects the batteries in order to use it as a load or as a back-up unit. More precisely, the batteries are recharged from the solar energy when the energy from the renewable source is higher than the energy consumed by loads and again the switch from battery to loads is also closed when the energy production of the photovoltaic system is not enough. As a result, the battery helps the photovoltaic system by matching the best configuration between the two generation sources on site.

The four batteries are connected in series and work at a nominal voltage of 48 V_{DC}. The type selected at The Green Village by *Victron Energy Blue Power* is lithium-ion battery, see Figure 15. Their rated capacity is 90 Ah, circa 5 kWh.

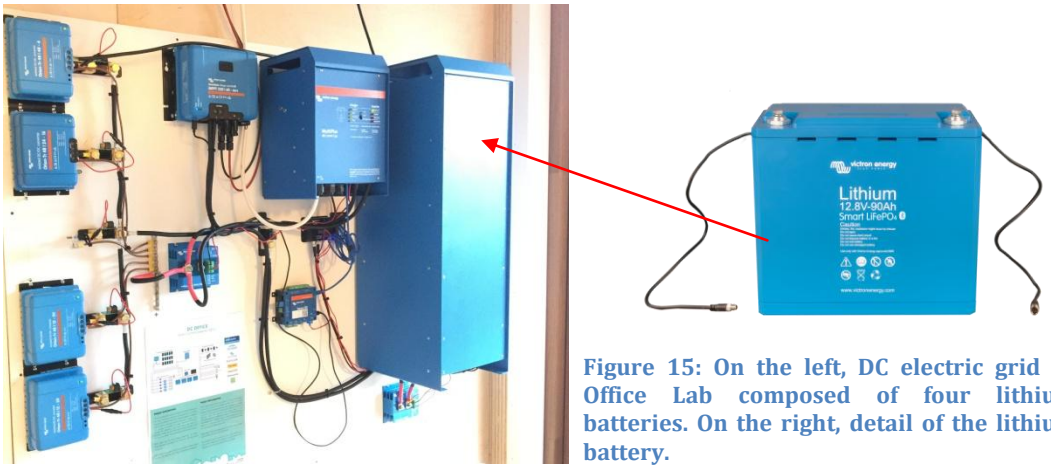

Figure 15: On the left, DC electric grid at the Office Lab composed of four lithium-ion batteries. On the right, detail of the lithium-ion battery.

The battery model works on Simulink as a dynamic model with a controlled voltage source, as shown in Figure 16. The voltage is calculated at each time step depending by the maximum battery capacity, polarization constant, low-frequency current dynamics and current; the latter factor is positive if the battery is discharging and negative when battery is charging. The minimum value of State of Charge in the batteries is selected to 20% in the first accurate model because the idea is to consider the worst case scenario in the average day of the month in order to take into account the chance of complete discharge in the batteries. It is worth to say that this parameter is lower than the real value set in the batteries. The maximum State of Charge is fixed to 90% in order to avoid overcharge in the batteries.

$$V_{discharge}(i > 0) = V_0 - K\frac{Q}{Q - i_t}i - K\frac{Q}{Q - i_t}i_t + A\, e^{-B \cdot i_t} \quad (5)$$

$$V_{charge}(i < 0) = V_0 - K\frac{Q}{i_t + 0.1 \cdot Q}i - K\frac{Q}{Q - i_t}i_t + A\, e^{-B \cdot i_t} \quad (6)$$

Equations (5) and (6) describe the discharge and charge model for the lithium-ion battery type. The maximum battery capacity Q is measured in [Ah]; V_0 is the constant voltage in the battery, A and B are the exponential voltage in [V] and [Ah]$^{-1}$ respectively; i is the low frequency current dynamics in [A] and i_t is the extracted capacity in [Ah]; K is the polarization constant in [Ah]$^{-1}$.

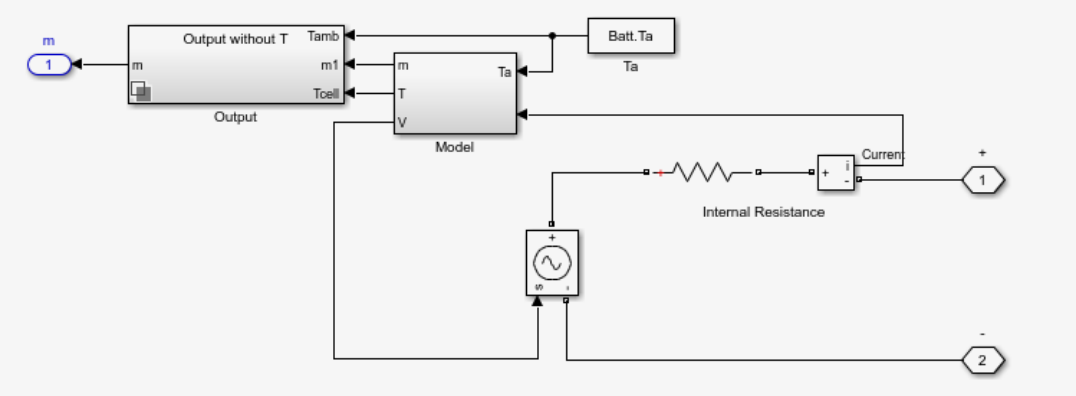

Figure 16: Equivalent circuit of rechargeable battery.

DC loads are simulated as resistive loads: in particular, the 48 V line is equipped with laptop and lighting system, while the 350 V line works only for heating purposes, until now. Their power consumption is set by *Engie* as 280 W in the lighting system, 1000 W as the maximum power in the infrared panels and 1000 W maximum output power of IT devices.

The three-phase inverter DC/AC consists of six power switching devices connected in an IGBT/diode bridge configuration, as in Figure 17.

The power converter works depending on the voltage and current values in AC and DC grids. First, the controller minimizes the fluctuation in the DC voltage due to changes in weather condition using PI controller; in the meantime, the Phase Locked Loop block synchronizes three-phase sinusoidal signals on a set of variable frequency which minimum is 45 Hz. After that, the current regulator takes the command current from the DC voltage regulator and compares with the grid current. Ultimately, the Pulse Width Modulated block generates three-phase signals to the IGBTs based on the required reference voltage.

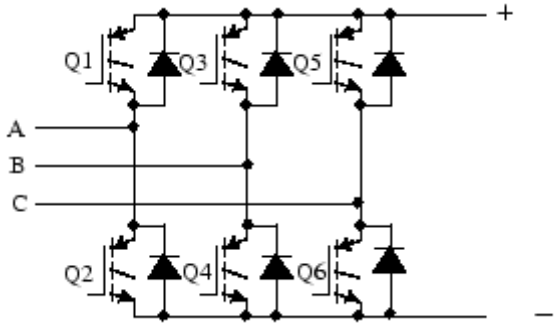

Figure 17: Three phase inverter DC/AC with IGBT- diode bridge. (36)

After all, the PV power plant implements a sinusoidal L-C filter, that is on the right in Figure

10. It is composed of inductors and capacitance.

3.2.2. 2nd fast analysis: Photovoltaic systems and batteries

The second system is modelled in order to have a faster response than the system described above, in the previous Paragraph 3.2.1. 1st accurate analysis: Photovoltaic systems and batteries

The main components are the same as in the first analysis, except the utility grid; there are two photovoltaic systems and four batteries, as presented in Figure 18.

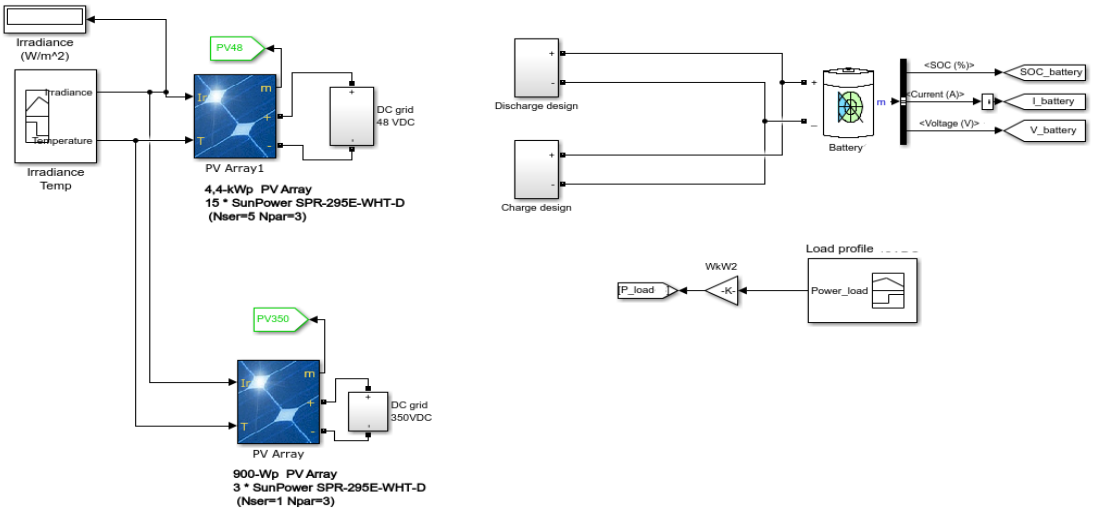

Figure 18: Compact scheme of the second model in Simulink.

The inputs are defined as in the previous case study and also the configuration parameters are the same. The main difference is that the solar energy systems, loads and batteries are not physically connected as in the first accurate model. Thanks to this solution, the simulation runs faster than before; the results of an entire month are collected always in less than five minutes, sometimes also in few seconds.

The energy balance in supply and demand is studied using a control file on Matlab. The algorithm takes weather conditions and load profiles as inputs in both the voltage lines. Consequently, the solar production is compared to the load consumptions at each time step. If the energy production exceeds the consumption, the electric circuit of batteries is closed which means that batteries are connected and charged until they reach their maximum limit of 90% state of charge if possible. In the opposite way, the battery circuit is again closed but this time batteries are discharged, if loads are not fully charged by solar panels. The minimum value of State of Charge in the second fast model is set to 30%, more realistic value if compared to the same parameter in the fist simulation, in order to avoid damaging the storage bank by excessive discharge during the whole year. The Matlab file controls at each time step the lower and upper state of charge of batteries as well, in order to protect them from over-charging or over-discharging.

3.2.3. Integration of hydrogen technology

One more goal of the simulation is to measure how much hydrogen could be produced per electrolysis using the excess of energy of the solar system in the low voltage line.

The idea about the integration of hydrogen technologies has changed during the study, mainly because of the meteorological condition in The Netherlands which cannot guarantee a big excess of electricity during all the year. The first plan was to implement the system on

Simulink and connect some fuel cell electric vehicles in order to avoid the excess of energy sent to the national grid and in order to supply energy, when it is needed in the office, without taking it from the utility grid. Whereas it was clear thanks to the first results in the simulations that the photovoltaic panels were not able to feed completely the loads in the office and at the same time the electric cars, the project was changed. Thus, before starting the simulation, the study considered the integration of fuel cell lightweight vehicles. In this case, the pressure in the storage decreases from the typical value in hydrogen car of 350 bar or 700 bar to just 10 bar. Moreover, the required amount of hydrogen in the two vehicles is considerably different. The hydrogen in gaseous form is stored in cars using two onboard tanks with around 6 kg of compressed hydrogen (24), while two metal hydride hydrogen canisters of 45 g each are used in hydrogen scooters. (37)
Some relevant features of the fuel cell lightweight vehicle are shown in Table 2 to appreciate the powerful of the device.

Scooter Fuel Cell system specification by APFCT	
Maximum Speed	>45 km/h
Type of Fuel Cell	PEM
Rated Voltage	24 V
Rated Power	1800 W
Operating Voltage	22-33 V
Operating Temperature	5-55 °C
Canister capacity	45 g
Number of onboard canisters	2
Cooling solution	Water

Table 2: Hydrogen scooter characteristics. (37) (38)

In the first hypothesis, the excess of energy should be calculated using the results from the accurate model, in which the hydrogen device could be integrated into the system as a new block on Simulink. It has to be considered that the only simulated day in each month runs the worst case scenario in which battery starts always the simulation with the lowest value of the state of charge equal to 20% at the beginning of the day. As a result, no excess is recorded during one of the twelve days. Therefore, the second model is crucial for measurements in both storage solutions: charge and discharge cycles in batteries and hydrogen production. The calculation of hydrogen is structured as described in the following steps:

- The first priority is the load electric consumption;
- The excess of renewable energy and its time span are recorded in each day of each month;
- The size of the electrolyser is determined by the value of available power;
- The hydrogen flow rate is calculated by Equation (7):

$$n_{H_2} = \frac{1}{2F} \cdot MW_{H_2} \cdot \frac{P}{V} \qquad (7)$$

  in which n_{H_2} is the hydrogen flow rate in $\left[\frac{kg}{s}\right]$, 2 is the number of electrons transferred, F is the Faraday constant equal to 96485 C, MW_{H_2} is the molecular weight of hydrogen
- The hydrogen scooter fleet is modelled according to the results in the previous steps.

3.3 Model assumptions and inputs

The solar systems inputs are taken from the website Royal Netherlands Meteorological Institute (KNMI) (29). The irradiance levels are recorded in the weather station situated in Rotterdam Airport, less than 5 km far from The Green Village.
One other value is required as input, the cell temperature. The efficiency is negatively influenced by cell temperature, especially during summer conditions.

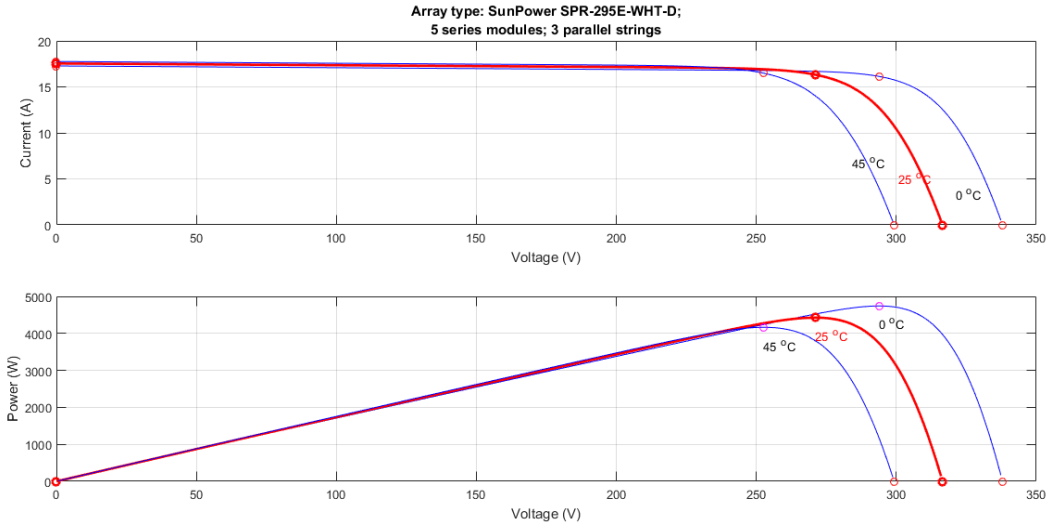

Figure 19: I-V and P-V characteristics of PV array in case of 1000 W/m² solar irradiance and different cell temperatures (0°C, 25°C and 45 °C).

The typical operating temperature in the system usually is higher than outside temperature due to many factors like solar irradiance, wind speed, thermal resistance and heat transfer coefficient of materials in the modules. All these factors affect the conduction and convection losses. Mainly, when PV modules are mounted on a roof, heat transfer could be different between back and top layers in the panel which could result in higher operating temperature. In the two graphs below in Figure 19, the temperature effect is shown for the 4.4 kW_P PV system composed by 15 panels.
The cell temperature is not measured in the photovoltaic system installed at The Green Village. Hence, the value is calculated starting from the hourly outside temperature and adding a constant of +5°C each day in order to consider possible overheating in the worst case scenario.
In the first accurate model, the state of charge in the battery is supposed to be equal always to the minimum value, 20%. This choice is based on a prudent assumption which led to an underestimation of the charging pattern each month. The idea is to check if the batteries can be charged from minimum to maximum state of charge during the simulated day in the month. Conversely, the second model is able to take into account the effect of more sunny or cloudy days in a row. Thus, the minimum State of Charge is set to 30%, more realistic value. The second simulation runs the first day in January with the maximum state of charge in batteries equal to 90%, as they are completely charged at the beginning of the analysis. The response time in the Lithium-Ion battery is set in the scale of microseconds.
It is worth to say that eventually the first model runs just one monthly averaged day in two months. This decision is taken mainly because of two reasons. The load consumption in the office is based on assumption because the real measurements of the DC grid at Office Lab are

started at the beginning of February 2018. It means that it would be small differences in assumptions of load profiles between two consecutive months. Furthermore, the solar irradiance variation is more significant if it is studied in this way. The second reason is faster simulations. Hence, it is chosen to collect data only in odd months for the first simulation.

3.3.1. DC loads profile

The DC load profiles in the simulations are assumed, whereas the measurement of the DC grid installed at the Office Lab started to be collected in February 2018.

The Green Village team is monitoring the office on the website *Climatics* (32). The data collection of AC consumption began in November 2017. It measures parameters through sensors like room temperature, relative and absolute humidity in the air, fan speed, electric current or power consumption (in AC).

In order to make right choices about electrical consumptions in the simulated microgrid, the recorded AC power consumptions are considered as the upper limit of the assumed DC load profiles, at least in the four months when the data are available (from November 2017 to February 2018). The DC consumptions are based also on the examination of other parameters, such as weather condition during the year, the total amount of sun hours, the day of the week and, in detail, which hour is in the day. The working hours in the office are from 8:00 to 19:00. All the electrical loads in the two meeting rooms are assumed always zero at lunch, because the two rooms are not used for a couple of hours.

DC loads are studied as lighting system, heating system and electrical outputs to connect laptops, phone chargers, monitors and other IT devices. In the low voltage line, the DC loads are LED lamps and IT output; the maximum power consumption is 280 W and 1000 W, respectively. The electrical plugs are assumed never at their maximum. The heating system is connected to the high voltage line; its maximum consumption is 1000W and it is used rarely at its maximum. Furthermore, during winter the heating system consumes much more in the first hours on Monday because during the weekend the Office Lab does not heat up the building and so the indoor temperature reaches very low temperatures, below 15 °C.

Table 3: Some DC load assumptions in both voltage lines in [W]. The low voltage line 48 V_{DC} includes lighting system and USB electrical output; while the high voltage line 350 V_{DC} just the heating system.

	January			April			July			November		
	$48V_{DC}$	$350V_{DC}$		$48V_{DC}$	$350V_{DC}$		$48V_{DC}$			$48V_{DC}$	$350V_{DC}$	
08:00	280	1000	**February = January**	280	0	**August = July**	280		**December = November**	380	500	
09:00	280	500		280	500		300			380	200	
10:00	380	300		380	150		280			0	0	
11:00	100	0		380	100		300			380	0	
12:00	100	0		0	0		0			0	0	
13:00	0	0		0	0		0			0	0	
14:00	0	0		0	0		0			0	0	
15:00	480	200		380	200		300			300	0	
16:00	380	100		280	0		0			300	0	
17:00	380	0		280	0		0			300	0	
18:00	280	0		280	0		280			300	0	
19:00	0	0		0	0		0			0	0	
20:00	0	0		0	0		0			0	0	

It is worth to say that DC load profiles are slightly different in the two simulations because

the first model has to consider the average monthly load consumption taking into account that during the weekend the DC loads are assumed totally switched off. Thus, the load consumptions in the second simulation are bigger than the same profiles in the first simulation during the same month. Moreover, some consecutive months present equivalent hourly report due to lack of more information, like January and February or July and August, see Table 3.

4. Results and discussion

The final results of both simulations are presented and discussed in this chapter. It presents the main outcome in each month. As explained above, the accurate analysis describes just one day in odd months; that day is obtained as a monthly average day in which the irradiance levels and cell temperatures are calculated each hour as mean values between the same hours each day during the entire considered month. It should be reminded also that the cell temperature is increased by +5°C. The reasons for these choices, assumptions and description of the case study are explained in Chapter 3.
As an alternative, the fast analysis runs all year in order to study the annual performance of the microgrid.
According to understand clearly the results obtained, it is important to remind that the differences between DC loads in the two different voltage lines is clarified in Paragraph 3.1. Microgrid description and boundaries. Load profiles are assumed each month, due to lack of more information. Many parameters are considered during the choice of load consumptions; among them, the seasonal time is the reason for the biggest changes. Clearly, in the high voltage line, the heating system is gradually switched off starting from the highest consumption in January to May and vice versa from September to December. Similarly, in the low voltage line the lighting system is used less and less from winter to summer because of more hours of sunlight in a day, and vice versa from summer to winter; while the charging pattern of IT devices is not influenced by this factor.
Furthermore, the second most important parameter in the structure of load profiles is the hour of the day. When the office is opening, the heating system is always switched on in winter. Its maximum capacity in the early hour of the day is chosen depending on the month analysed and more in detail, the outside temperature. In the low voltage line, load profiles present each month peak in consumption after lunch when it is assumed that everyone comes back to the office to work.

The sign convention is well described in Paragraph

3.2. Simulation on Matlab/Simulink.
The main results are organised in the following way:

- the accurate model is studied in four graphs. First, the power production is analysed in the two photovoltaic systems. Then, DC loads in both systems are compared to solar production and, when necessary, the connection to the utility grid is analysed. Ultimately, the state of charge in batteries is measured;
- the fast simulation results are plotted in figures about monthly inputs in terms of irradiance and temperature levels, solar power production in both systems, balances between production and consumption in both systems (utility grid is not simulated as

a block, but the interface between the microgrid and the AC grid is extrapolated as a further *a posteriori* analysis).

4. 1. January 2016

In January, the irradiance levels are strongly reduced because of cloudy days. If clear sky conditions are considered, the database PVGIS reports a peak around 230 W/m² of average daily solar irradiance considering optimal panels position and inclination. Conversely, real data are recorded by KNMI and they reflect only half of the value registered by PVGIS. As shown Figure 20, at least seven days are completely covered by clouds with just barely 20 W/m². The highest value is slightly above 100 W/m² in four days.

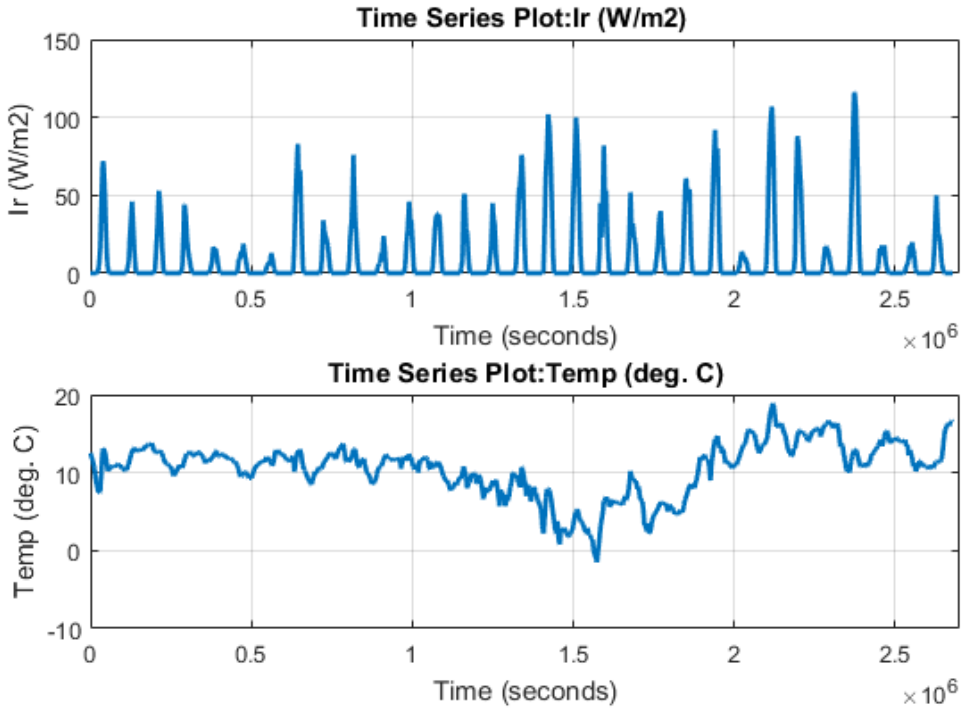

Figure 20: Solar PV inputs in January 2016. The above graph describes the irradiance levels during the month in [W/m²]; the graph below shows the temperature variation in [°C] during the month.

Whereas the average day in the first model takes into account the monthly variation, the peak in irradiance value is 50 W/m² at noon.

The sunrise is around 8 am; while the sunset around 5 pm. Thus, the photovoltaic panels work 9 hours per day, approximately.

4.1.1 First simulation results

Figure 21 shows the solar production in both voltage lines, in which both power curves reflect the monthly average irradiance. Clearly, the power production is lower than the nominal value of 4.4 kW_P or 0.9 kW_P during the winter season.

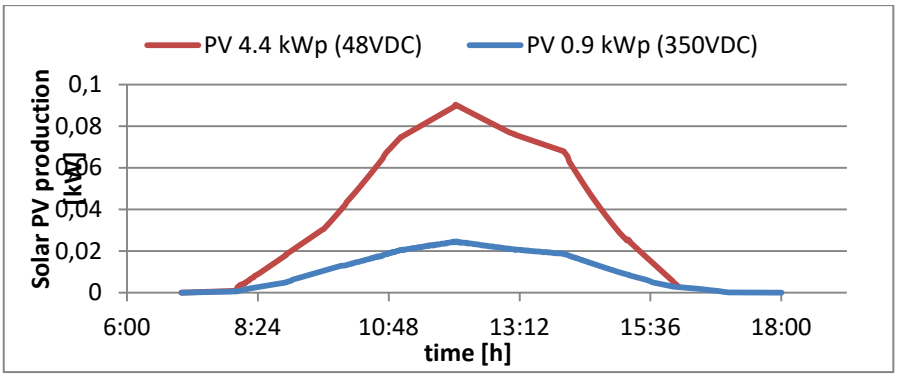

Figure 21: Daily PV panels production in January 2016 (first simulation).

The energy balances in the voltage lines are resumed in Figure 22 and Figure 23.
As expected, the grid connection is fundamentally required in January because the solar production is too low in both systems. Solar production is even not visible in Figure 22 because of its low value.
Figure 22 shows the high voltage line 350 V_{DC}. DC loads (IR panels) are connected from 9 am to 11 am and then one more hour at 3 pm, after the lunch break. The highest consumption is 1000 W recorded in the early morning when the office is opening because the temperature usually decreases from 24°C to 18°C during the night, as registered in the Office Lab using the website *Climatics* (32). Even more is the temperature reduction during the weekend, when the room temperature is often below 15°C in January. The consumptions in the two other time slots are 250 W and 200 W, respectively.
Thus, the smaller solar system tries to feed the DC loads, when it is required, even if in winter the solar production is low; as Figure 22 shows the green curve of the PV system is nearly zero compared to the consumptions. Conversely, when the loads are switched off in the microgrid, the solar production is sent to the utility grid as exported energy. These energy transfers are the result of no storage solutions integrated in the high voltage line.

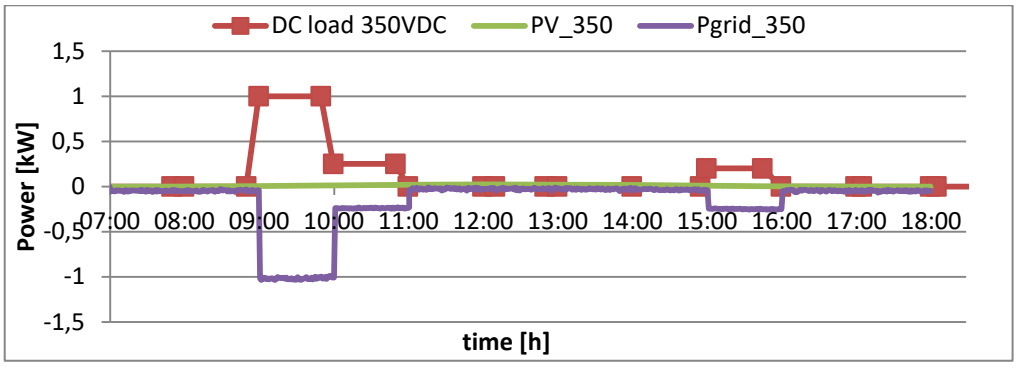

Figure 22: Daily energy balance in the high voltage line 350 V_{DC} (January, first simulation).

DC loads in the low voltage line, 48 V_{DC}, are studied in Figure 23. LED lights are always switched on during the day, except from 12 pm to 3 pm. The highest consumption is recorded at 3 pm, when lights and some IT devices are connected; it is equal to 480 W. It is assumed that the Office Lab closes at 6 pm in winter. There are some power fluctuations when the DC grid is connected to the utility grid twice: in the morning for the first 15 minutes and also when the power consumption varies in the afternoon because of quick power variation.
In the low voltage line, batteries are charged from 12 am to 3:10 pm, as shown in Figure 24. The state of charge achieves scarcely 21% before falling down due to load consumption.

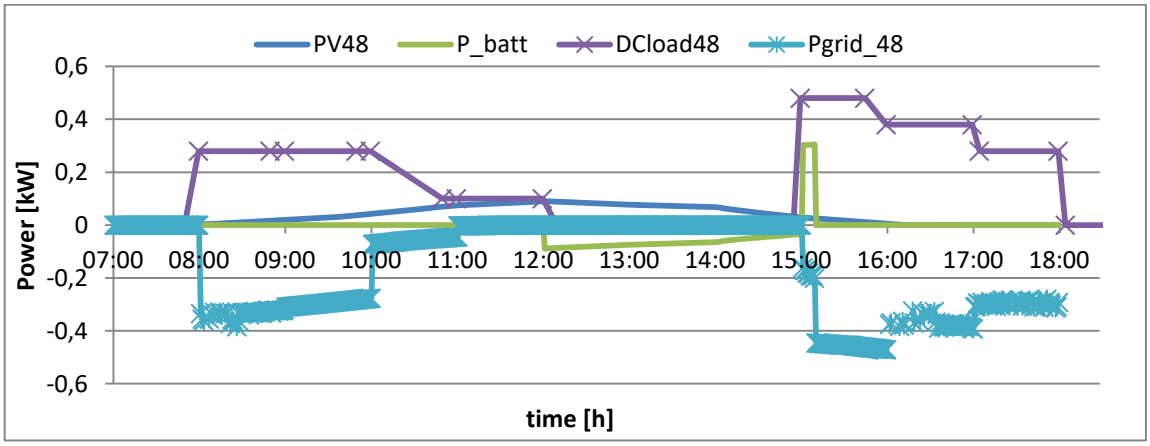

Figure 23: Daily energy balance in the low voltage line 48 V_{DC} (January, first simulation).

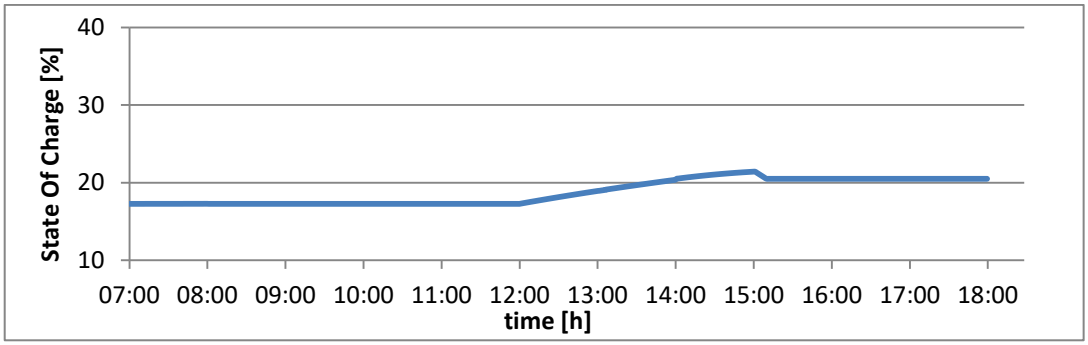

Figure 24: Daily variation in the State Of Charge of the batteries connected to the low voltage line (January, first simulation).

4.1.2. Results of the second simulation

As explained at the beginning of Paragraph 1. January 2016. , the weather conditions are adverse (in terms of solar production) in January and generally during the whole winter in The Netherlands. This fact causes very low solar production rate. More in detail, monthly solar production is shown in Figure 25 for both the voltage lines. The last graph in Figure 25 presents also monthly battery scheme of charging (when power is negative) or discharging (when power is positive), which is reflected on the state of charge, in Figure 26.

In January the batteries are fully discharged almost every workday; during the weekend, they are charged up to 35% or maximum 43% because DC loads are assumed off.

In January, the grid connection is necessary in order to feed the DC loads in the office.

Figures illustrate the monthly energy balance in the 350 V_{DC} voltage line in Figure 27 and in Figure 28, the 48 V_{DC} voltage line.

It is evident that the high voltage line cannot feed the heating system during winter without any connection to the main grid, see Figure 27. DC loads are represented by the yellow line; each Monday, the heating consumption is higher than the typical value during workdays because the temperature decreases often below 15°C during the weekend, as anticipated in Paragraph 1. January 2016.

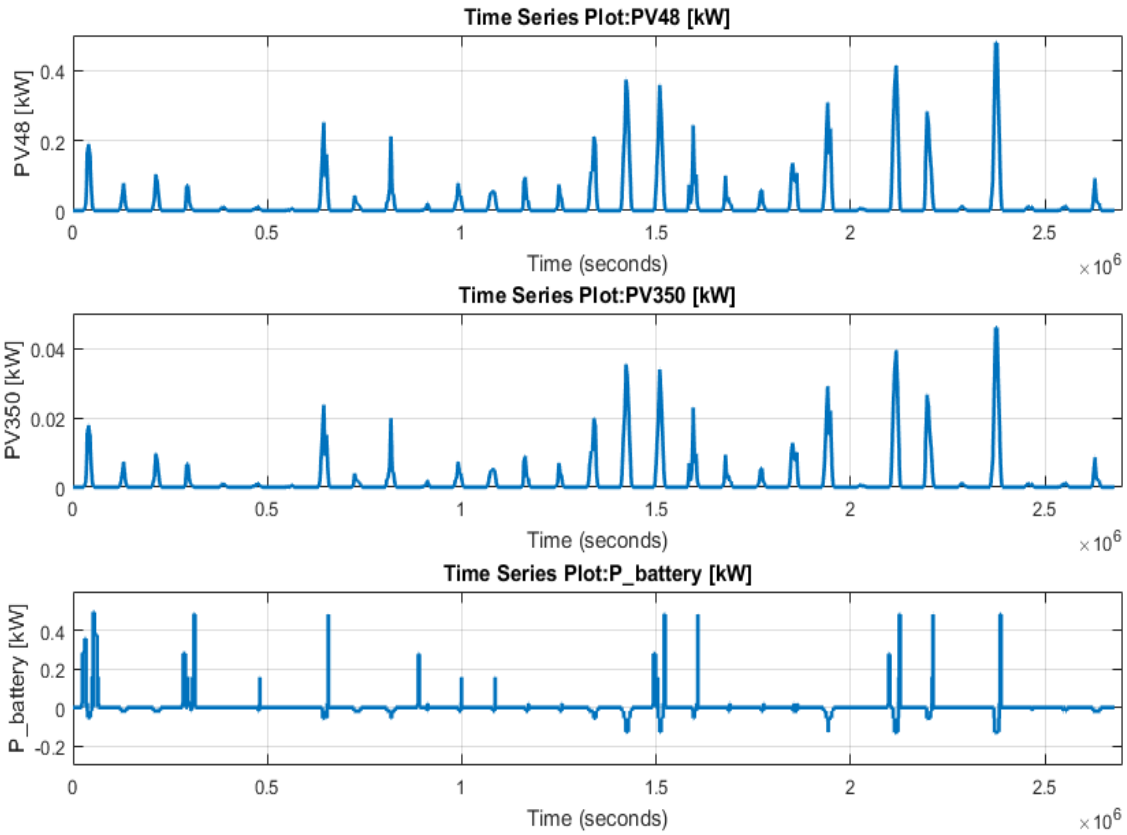

Figure 25: Monthly solar production in [kW] in the microgrid (January, second simulation). The first graph above represents the PV system in the low voltage line; the second one is the PV system in the high voltage line; the last graph is about battery charging and discharging scheme.

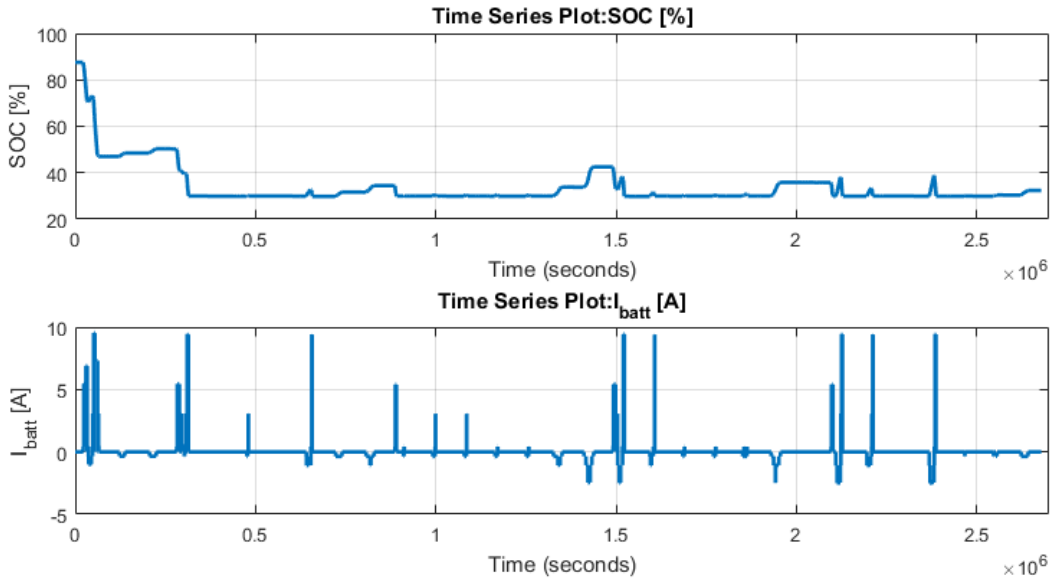

Figure 26: Battery performance in terms of the state of charge (graph above, in [%]) and current (graph below, in [A]). (January, second simulation).

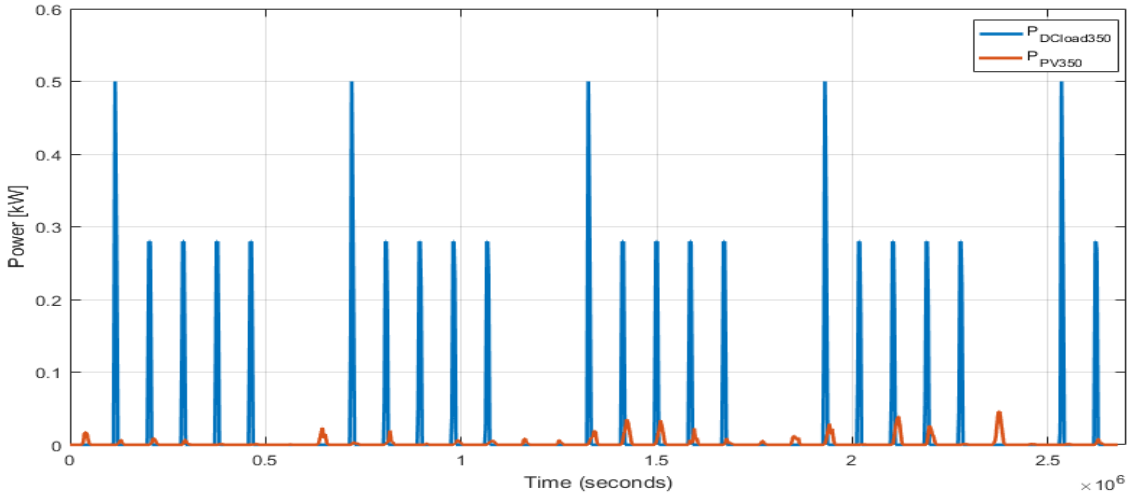

Figure 27: Monthly energy balance in the high voltage line (January, second simulation).

Monthly energy balance in the low voltage line is presented in Figure 28.

As described in the legend box in Figure 28, the yellow line is the photovoltaic power production that is always lower than loads consumption (blue line), except on January 28th. The battery system (red line) starts the simulation in January with 90% state of charge; but, due to low irradiance levels, batteries are discharged from 90% to 48% already in the first day. The negative values in Figure 28 correspond to an excess of power in the solar system. More in detail, the green curve is exactly the excess of power which is available to charge the batteries. Nevertheless, the charging scheme in batteries is slightly slower than the oscillation in the solar system. Thus, batteries cannot exactly move behind the instantaneous variation in the solar system. The charging scheme is built gradually, following the increase in available power, but in January it never reaches the maximum (negative) value.

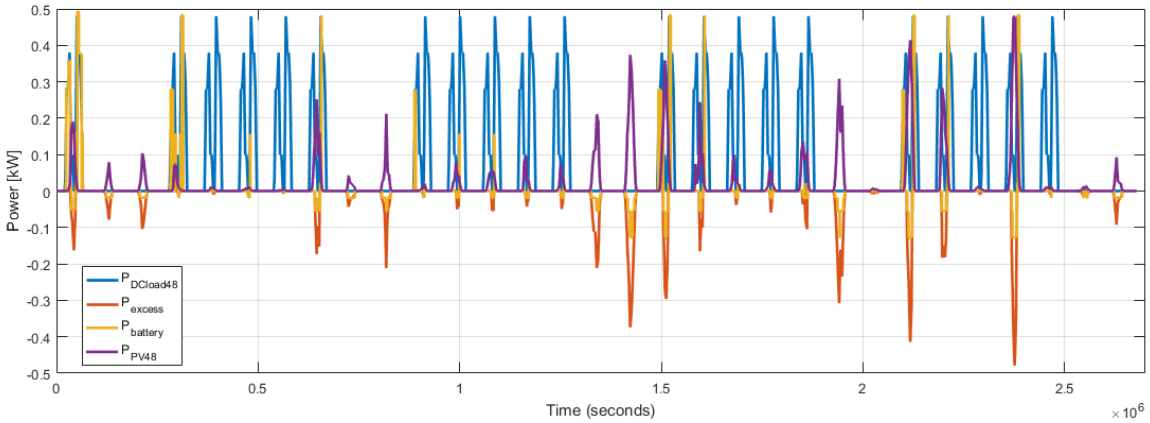

Figure 28: Monthly energy balance in the low voltage line (January, second simulation).

4.2. February 2016

As in January, the solar production at beginning of February is extremely low. In the first half of the month, it is always below 0.5 kW in the bigger solar system and lower than 0.05 kW in the smaller one.

In the second half of February, irradiance level is higher than the entire January and beginning of February itself, see Figure 29. The average solar irradiance in February is double compared to the same value in January; it reaches nearly 85 W/m^2 at noon during an average day. The solar hours increase as well in February; sunlight is available for 11 hours (two hours more than in January).

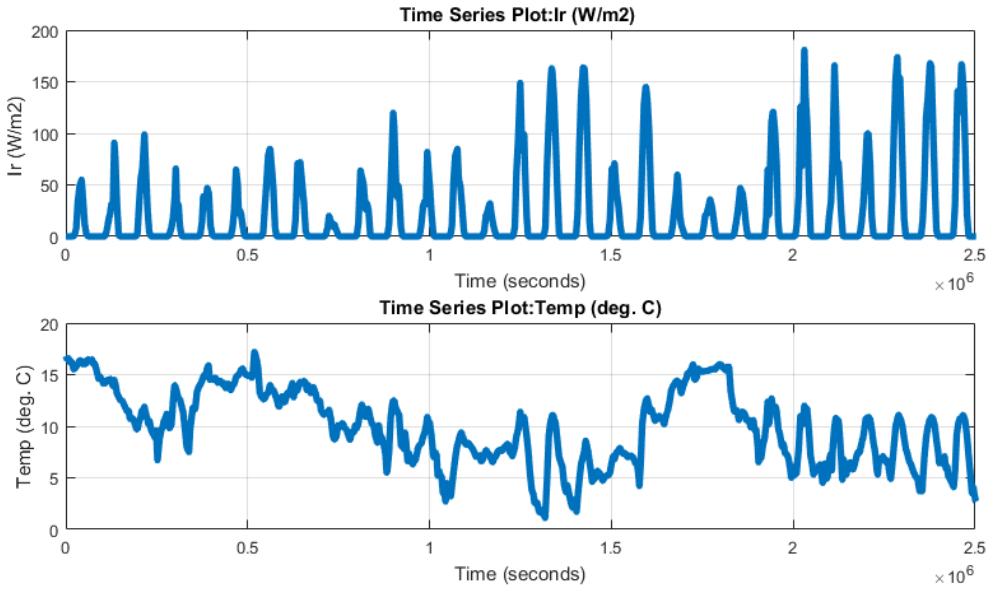

Figure 29: : Solar PV inputs in February 2016. The above graph describes the monthly irradiance level in [W/m²].

4.2.1. Results of the second simulation

The increase of inputs values results, of course, in an improvement directly visible in the solar production of both systems and consequently in batteries, respectively in Figure 30 and Figure 31. It is worth to say that surprisingly batteries in February achieve the maximum state of charge for the first time in the year, as presented in Figure 31. The 90% state of charge is achieved three times, on February 17th, 28th and 29th. More precisely, on February 28th and February 29th, there is an excess of energy for 11 h in total and it is sent to the grid as exported energy.

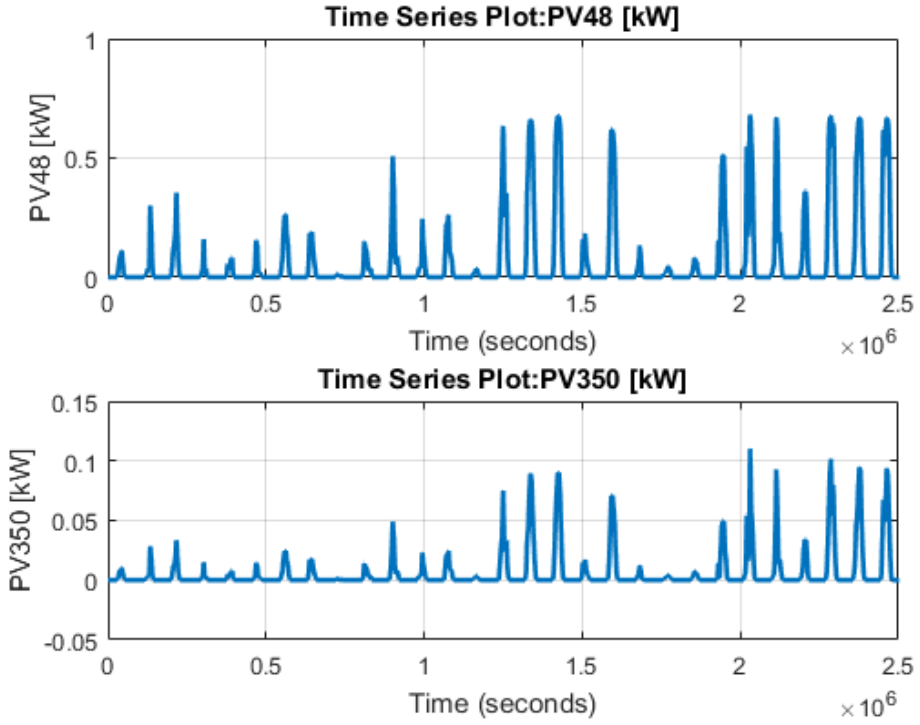

Figure 30: Monthly solar production in [kW] in both voltage lines, 48V_{DC} in the graph above and 350 V_{DC} below. (February, second simulation).

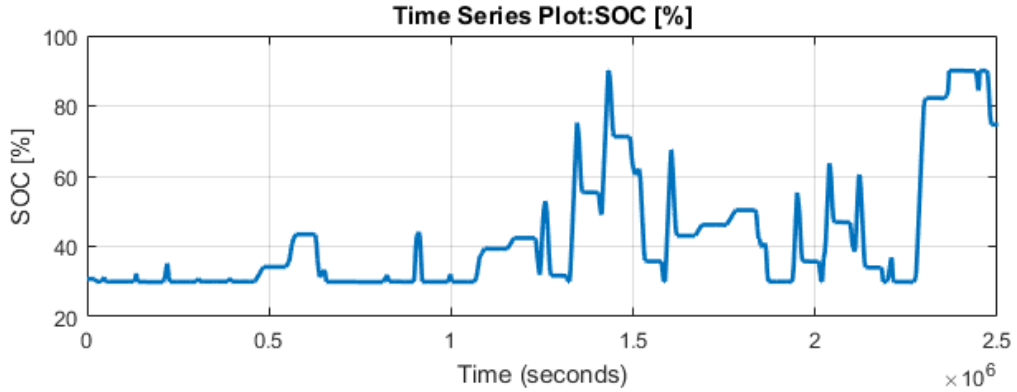

Figure 31: Battery state of charge in [%]. Time in the x-axis is in [s] (February, second simulation).

Load profile in February is assumed the same as in January due to lack of more information. Even if the solar production is slightly higher at the end of the month, the 350 V_{DC} voltage line needs still the grid connection to feed the DC loads, see Figure 32.

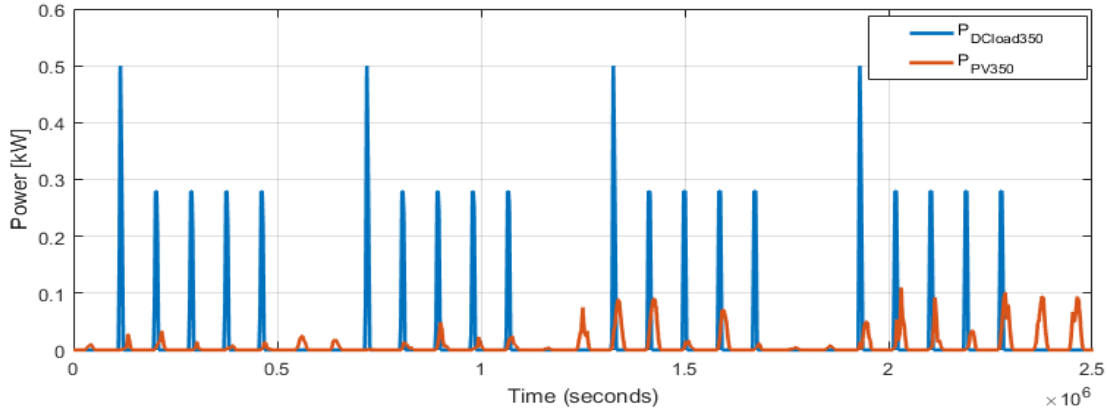

Figure 32: Monthly energy balance in the high voltage line (February, second simulation).

Energy balance in the low voltage line is shown in Figure 33. The red rectangular box in dotted line highlights the two days when there is excess in production of electricity.

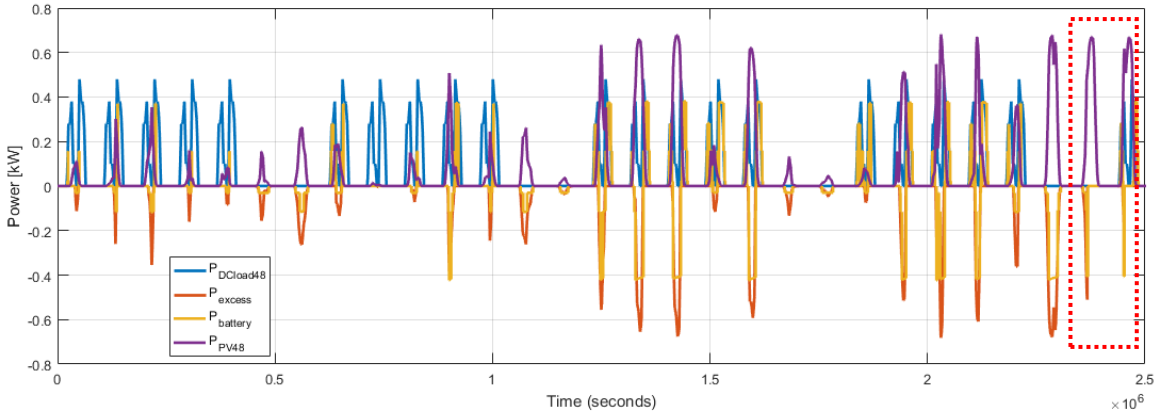

Figure 33: Monthly energy balance in the low voltage line (January, second simulation).

4.3. March 2016

Monthly solar irradiance variation is shown in Figure 34. Whilst there are at least four days that present the lowest irradiance level, around 50 W/m², grid supply is not necessary because those days are not in a row. Accordingly, the batteries could afford to feed loads during those days that are well spread over the month (March 1st, 4th, 15th and 18th).

It is evident that the best day in terms of solar production is March 30th, in which the solar

irradiance is higher than 250 W/m². Nonetheless, the theoretical maximum input value in clear sky condition is slightly below 500 W/m², as calculated by PVGIS (28).
In March, the sun is up from 7 am to 6 pm. If the solar irradiance was enough, PV systems could theoretically work without any connection to the main grid because the hours when the office is open are exactly in the same time span of the daylight.

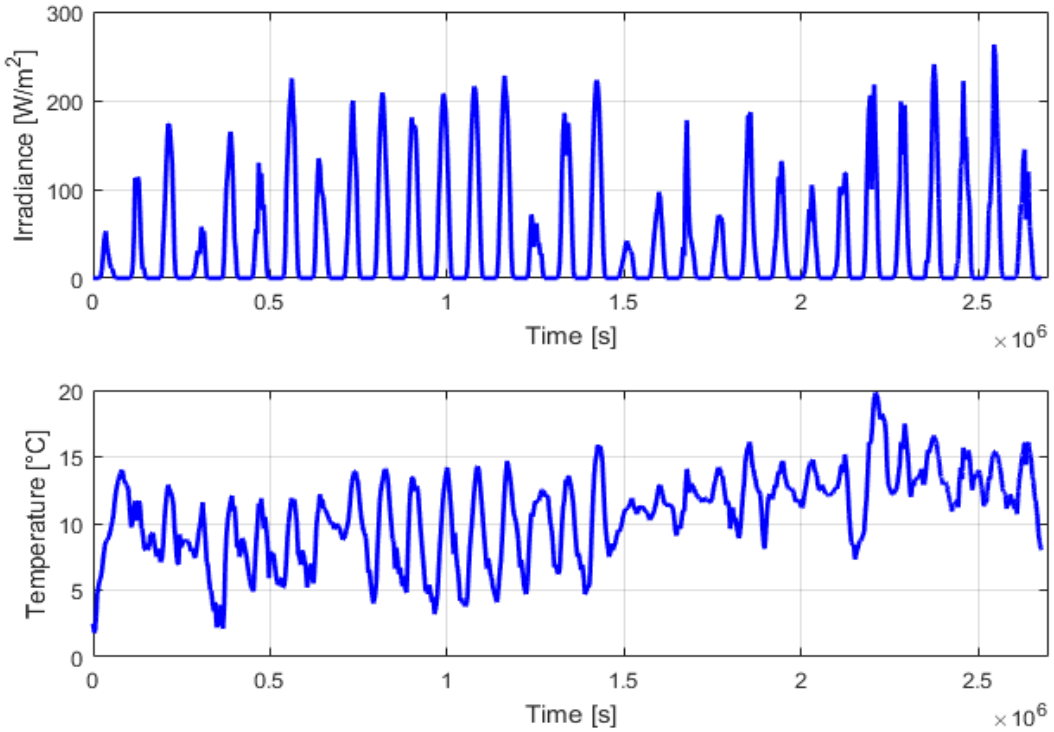

Figure 34: Solar PV inputs in March 2016. The above graph describes the monthly irradiance level in [W/m²]; the graph below shows the monthly temperature variation in [°C].

4.3.1. First model results

The assumption in the high voltage line during March is that the heating system is not used at its maximum output (1000 W) because the temperatures are increasing, even if during night hours the external temperature is often around 0°C.
The solar production is still too low in March, see Figure 35. Consequently, the utility grid is needed when loads are connected in the microgrid. On the other hand, when the heating system is switched off, the entire solar production is sent to the grid as an excess of electricity.

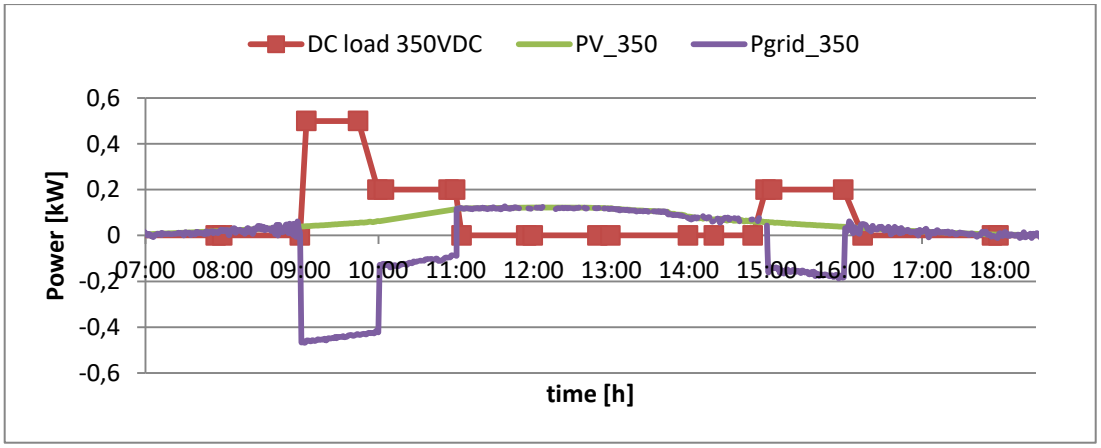

Figure 35: Daily energy balance in the high voltage line 350 V_{DC} (March, first simulation).

The highest consumption is 500 W at 9 am; then the heating system is turned on at 200 W for two more hours during the average day.
It should be noticed that the DC loads are fed by the solar system and the utility grid. This is the reason why the power delivery from the grid is not constant; it goes up or down close to the consumed power in DC loads because the grid supply has to be summed (in absolute value) to the solar production.
The comparison between production and consumption in the low voltage line is represented in Figure 36. The utility grid provides less than 200 W in the morning and less than 100 W in the late evening; thus the AC connection is still required in the system.
Whereas batteries are charged until a value higher than the lowest SoC during the peak hours of the average day, they work in the afternoon combined with the solar system to feed the DC loads. Eventually, batteries are almost totally discharged when the sun goes down; so, at the end of the day, the utility grid is again essential.
Even if the excess in the solar system is nearly 400 W for more than three hours, the batteries need more energy to reach the maximum charge, see Figure 37. The maximum value of SoC in March is 43.2%.

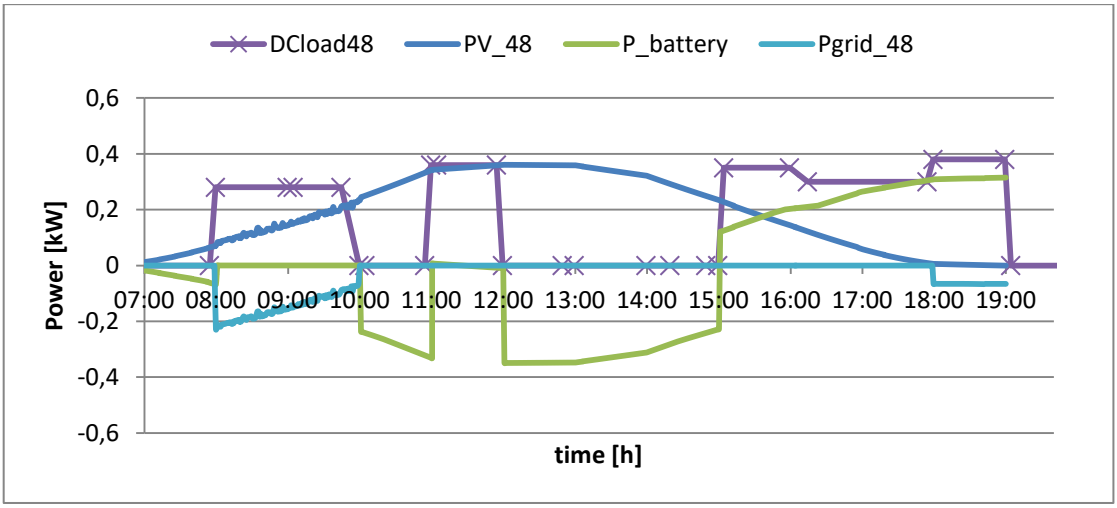

Figure 36: Daily energy balance in the low voltage line 48 V_{DC} (March, first simulation).

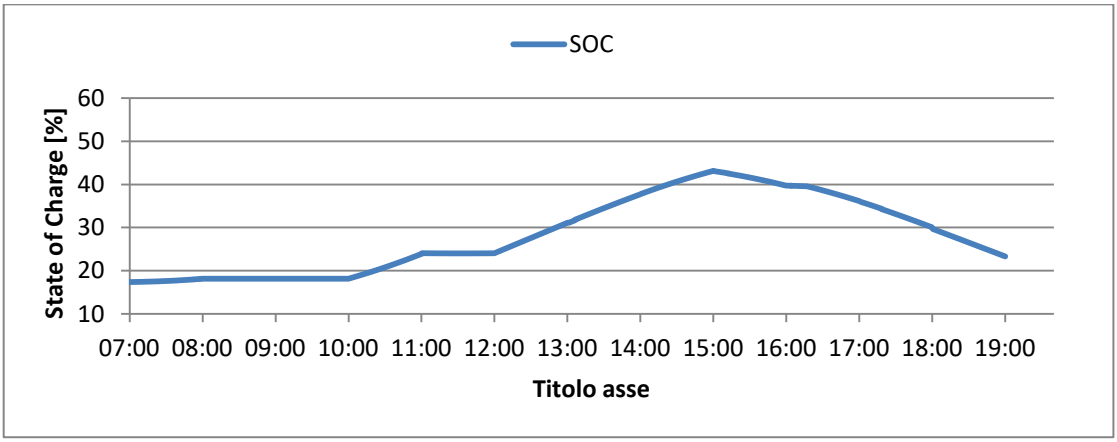

Figure 37: Daily variation in the SoC of the batteries connected to the low voltage line (March, first simulation).

4.3.2. Second simulation results

Monthly solar productions are shown in Figure 38, in which the four days with the lowest monthly solar irradiance are even more perceptible than previously in Paragraph sopra4.3.

March 2016

It is important to say that, as expected, the monthly solar production in both PV systems is similar to the results of the first model, if average values are considered. Whilst the first model works with average solar irradiance, the obtained daily solar production in the average day reflects the mean value of monthly solar production in both systems.

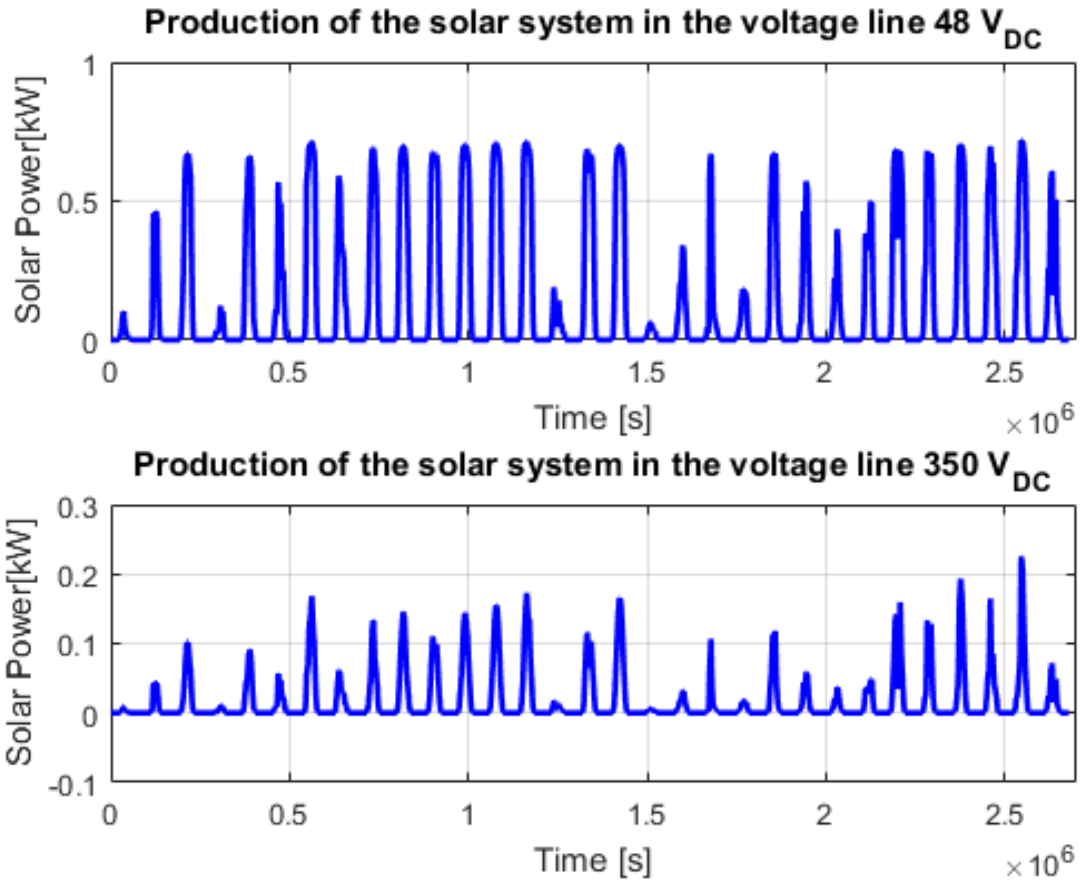

Figure 38: Monthly solar production in [kW] in both voltage lines: 48V_{DC} in the graph above and 350 V_{DC} below. (March, second simulation).

In the low voltage line, the maximum production in March is around 700 W per day. According to the maximum daily consumption around 500 W at 3 pm, the result is that the batteries are charged almost during all day. Indeed, Figure 39 shows that the state of charge is around 90% most of the time in March. More in detail, at the beginning of March the state of charge is 78% because of the resulting charging pattern in February. Then, it decreases from 78% to its minimum value until March 4th because of variable (and bad) weather conditions. Afterwards, batteries are always charged and never reach again the minimum state of charge, except in one day, March 25th, when the loads in the early morning combined to low solar radiation discharge the batteries for one hour and half.

A detail of the monthly balance is shown in Figure 40. The solar production is always higher than the power consumed in March. The result is that the batteries reach daily the full charge during the entire week in Figure 40, from March 6th to March 13th, except on March 9th. There is an excess of production (the yellow line is higher than the blue line) but batteries are off (red line at zero). That means that the excess is exported to the main grid (not represented).

Whilst the 48 V_{DC} is nearly standalone thanks to batteries, the DC loads in the high voltage line need still the utility grid in order to work, see Figure 41. The solar production is well below the power consumption during workdays; while during weekends, all the production is

lost to the grid.

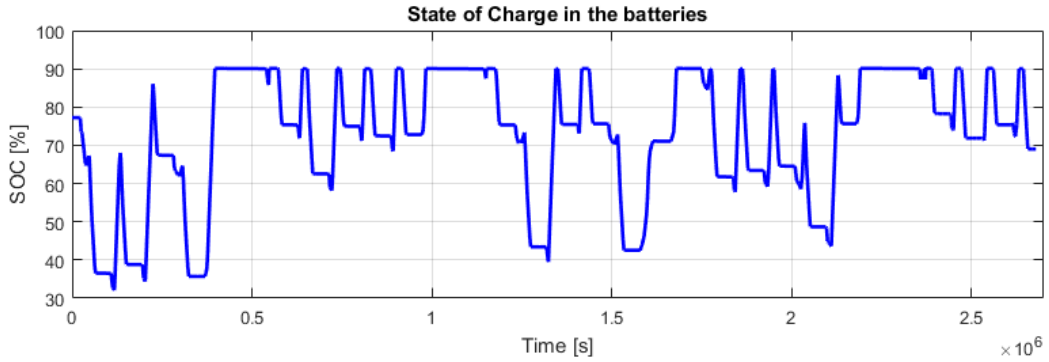

Figure 39: Battery state of charge in [%] (March, second simulation).

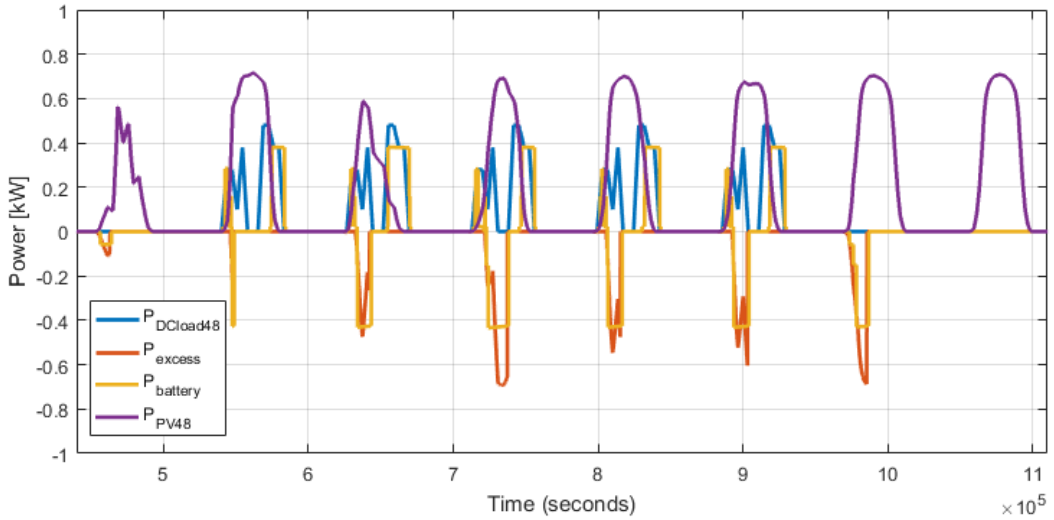

Figure 40: Energy balance in low voltage line (March 6th – 13th, second simulation).

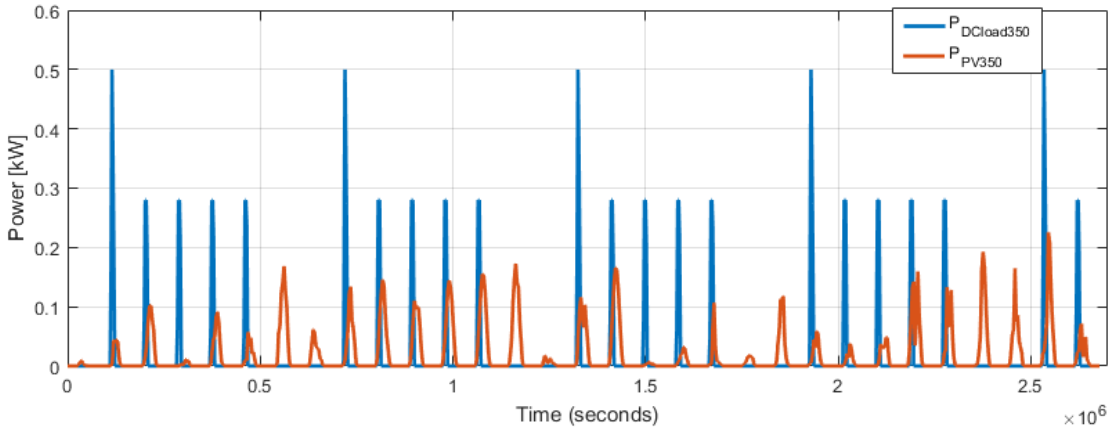

Figure 41: Monthly energy balance in the high voltage line (March, second simulation).

4.4. April 2016

April is not discussed extremely in detail like past months; only the most important and significant features are analysed.

Obviously, the solar production is improved in comparison to past months, but again the weather conditions could be even better. The recorded data of solar irradiance are less than half the value obtained in the best conditions. Anyway, Figure 42 presents just two days with the worst irradiance around 100 W/m², on April 6th and 25th.

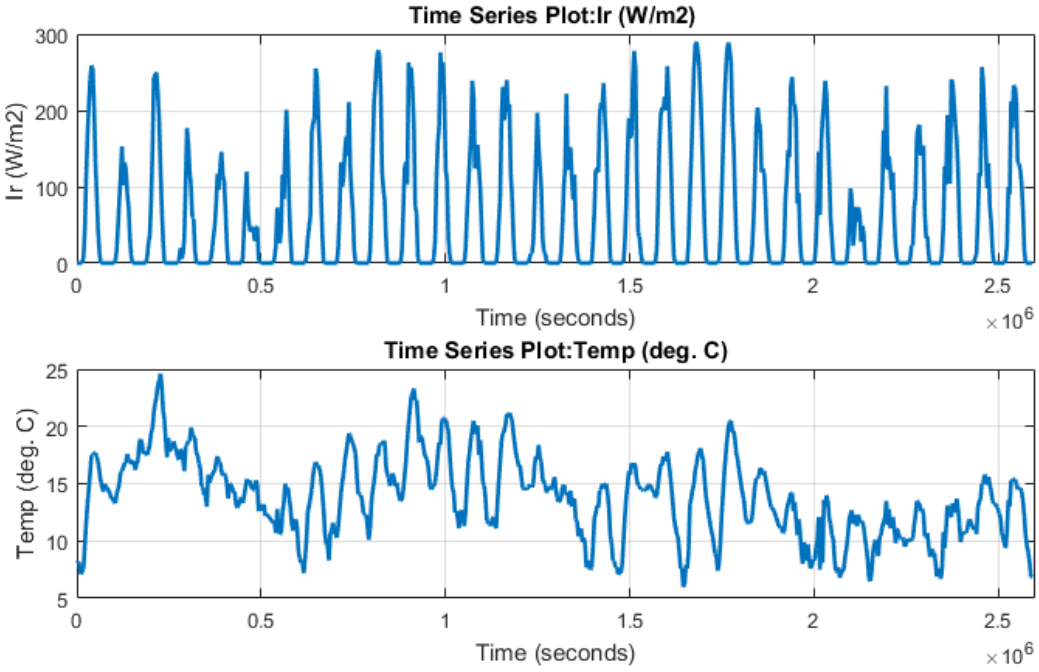

Figure 42: Solar PV inputs in April 2016. The above graph describes the monthly irradiance level in [W/m²]; the graph below shows the monthly temperature variation in [°C].

4.4.1. Second simulation results

Whilst the assumed consumption of the DC loads are decreased, the utility grid connection is still required in the high voltage line, see Figure 43. Conversely, the low voltage line could totally work without any connection to AC grid; batteries supply the loads when it is necessary and their state of charge is always higher than 50%, as shown in Figure 45.

It could be useful to analyse a detail of the monthly energy balance in the 48 V_{DC}. Figure 44 shows daily consumption and production on April 6th. The daily operating conditions are shown in order to understand how fast is the battery response in discharging scheme to feed DC loads and how the batteries are discharging according to the unpredictable solar production during the day.

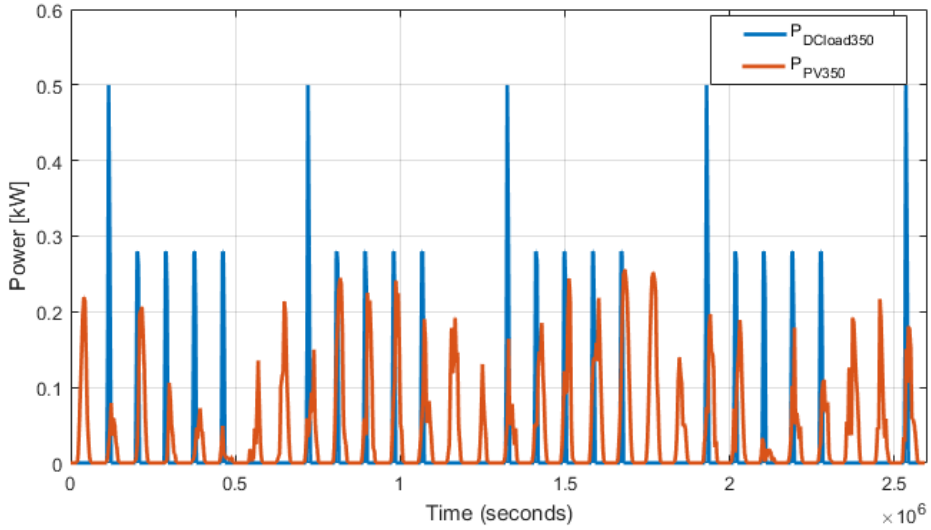

Figure 43: Monthly energy balance in the high voltage line. (April, second simulation)

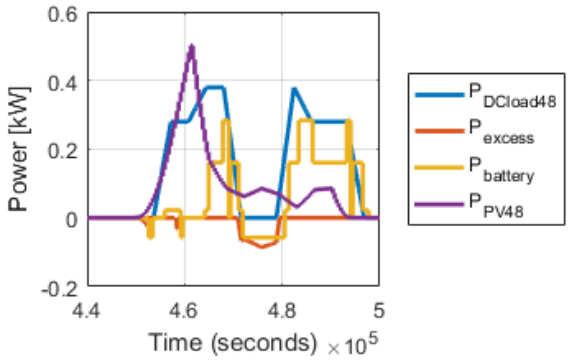

Figure 44: Daily energy balance in the low voltage line. (April 6th, second simulation).

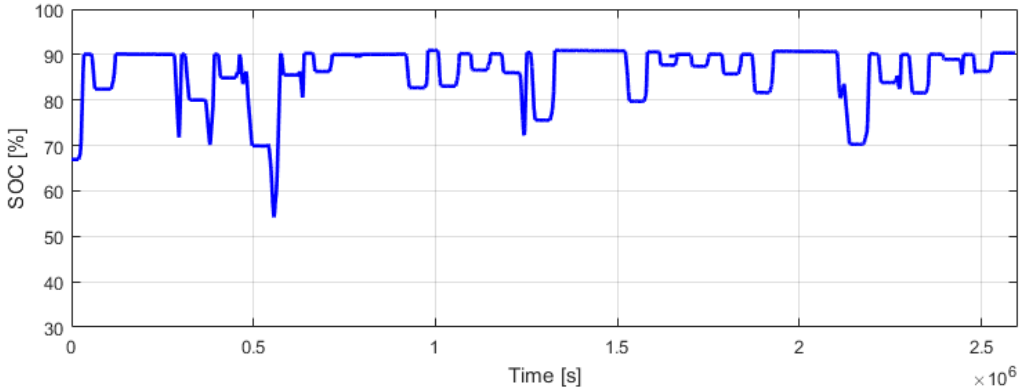

Figure 45: Battery state of charge in [%] (April, second simulation).

4.5. May 2016

The main important result in May is that the AC grid could be removed at all, in both simulations. Whilst the solar production is still below 1 kW, it is enough to satisfy the peak load demand which is actually very low. The heating system is assumed off during the summer period, from May to September, while the DC loads in the low voltage line consumed always less than 300 W in both simulations.

Monthly solar irradiance is comparable to April, see Figure 46. There are some bad days at the end of the month, but still the average input sent to the first simulation is quite high. Indeed the peak (average) value is at 11 am of 213.39 W/m^2.

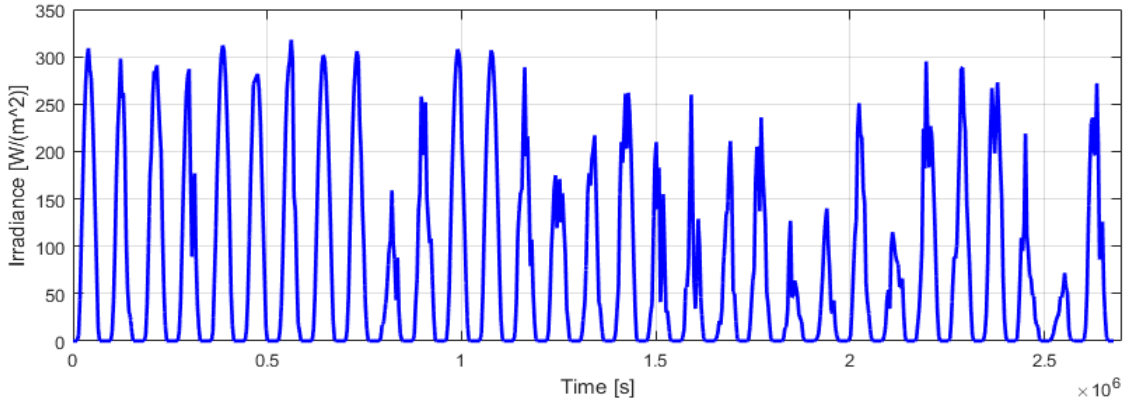

Figure 46: Monthly irradiance level in May 2016 measured in [W/m^2].

4.5.1. First simulation results

In Figure 47, load profile is always supplied by the combination of the solar system and batteries. Thus the main grid is not shown. The batteries are used at 3.30 pm to feed the loads

and at the end of the day to supply the lighting system (280 W) completely. They are charged for most of the time in the average day reaching 90% at 6 pm for less than ten minutes, as presented in Figure 48.

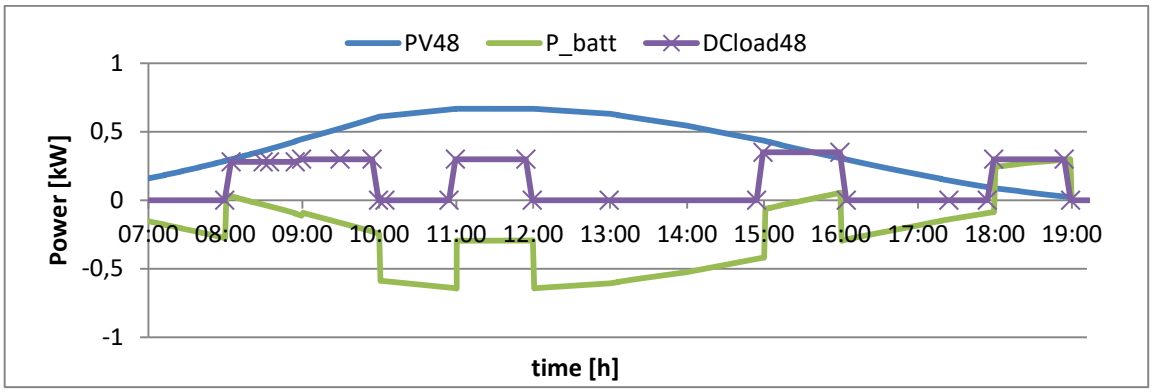

Figure 47: Daily energy balance in the low voltage line 48 V_{DC} (May, first simulation).

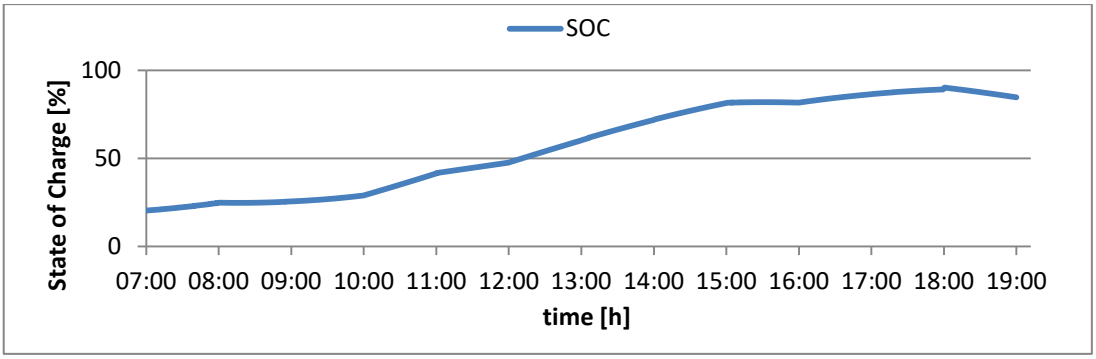

Figure 48: Daily variation in the SoC of the batteries connected to the low voltage line (May, first simulation).

4.5.2. Second simulation results

Results in the second simulation are quite the same as in April. It is worth to show the state of charge in batteries in Figure 49. It is always around 90%, except on cloudy days. The lowest value is reached on May 30th when batteries are discharged until 63%.

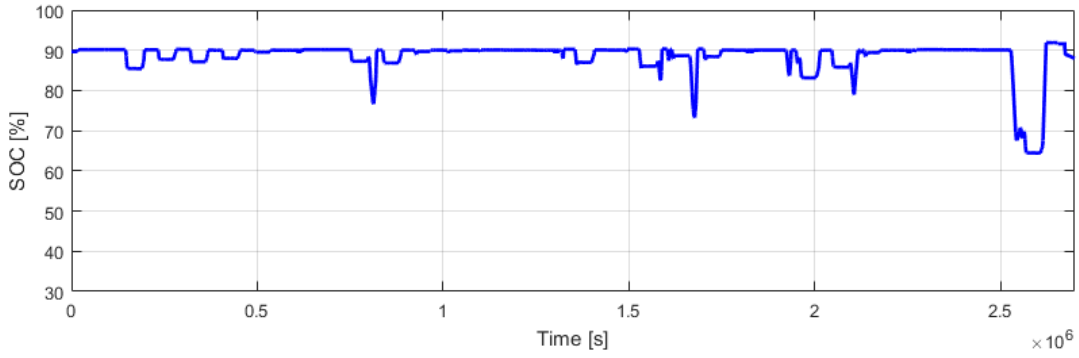

Figure 49: Battery state of charge in [%]. (May, second simulation).

4.6. June 2016

Results obtained in June are essentially equivalent to the two previous months. There are some cloudy days on June 2nd and some others in a row in the middle of the month, June 20th and 21st. Because of that, the charge in the batteries decreases from 90% to 53% on June 2nd and from 90% to 50%, the lowest value in the month, on June 21st.

4.7. July 2016

July confirms the same features of the past months with good weather condition. Whereas there is just one cloudy day on July 1st in which the solar irradiance peak is slightly above 50 W/m², the monthly average irradiance achieves the highest yearly value of 214.84 W/m² at noon. In some days the solar input is higher than 300 W/m² too.

The remarkable outcome of the first simulation is that the state of charge in the batteries is 90% for 30 minutes (from 5.45 pm to 6.13 pm).

The first day of the second simulation shows the worst condition, see Figure 50; the batteries are discharged straight from 83% to 64% on that day. Except for July 1st, their state of charge is quite often 90%.

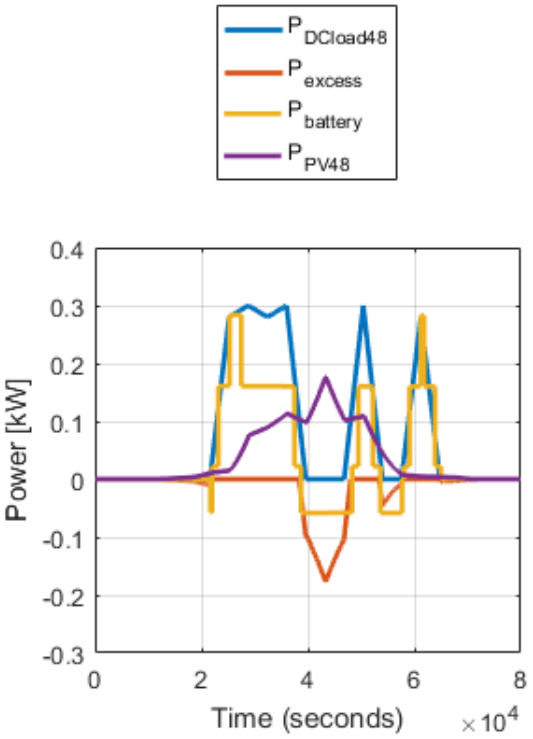

Figure 50: Daily energy balance in the low voltage line. (July, second simulation).

4.8. August 2016

An important detail of the simulation in August is that no summer holidays are considered. The grid connection is still unnecessary because batteries are fully charged almost every day in the month excluding August 2nd and 11th when the lowest state of charge is 60%.

4.9. September 2016

The peak of the average solar irradiance in September is 181.97 W/m²; it is almost equivalent to the one in June, but the daylight is quite reduced compared to June. Basically, the sun shines from 6 am to 6 pm. The monthly peak is instead 250 W/m²; it occurs just twice, at the beginning of the month on September 1st and 5th.

4.9.1. First simulation results

In September, the solar systems work less efficiently. After the maximum production of 0.7 kW in the past month, the solar production in September is lower and it is shown in Figure 51.

The heating system is still assumed off in September, thus the entire production in the smaller solar system is sent to the grid. For the first time after summer period, the low voltage line needs the connection to the utility grid in order to feed the loads, but only in the early morning when the batteries are not charged enough yet, see Figure 52. The main reason is that batteries start always the first simulation with no charge. In any case, the excess of energy during the day is still sufficient to charge the batteries from the minimum to the maximum value of 57% twice, at 3 pm and 6 pm.

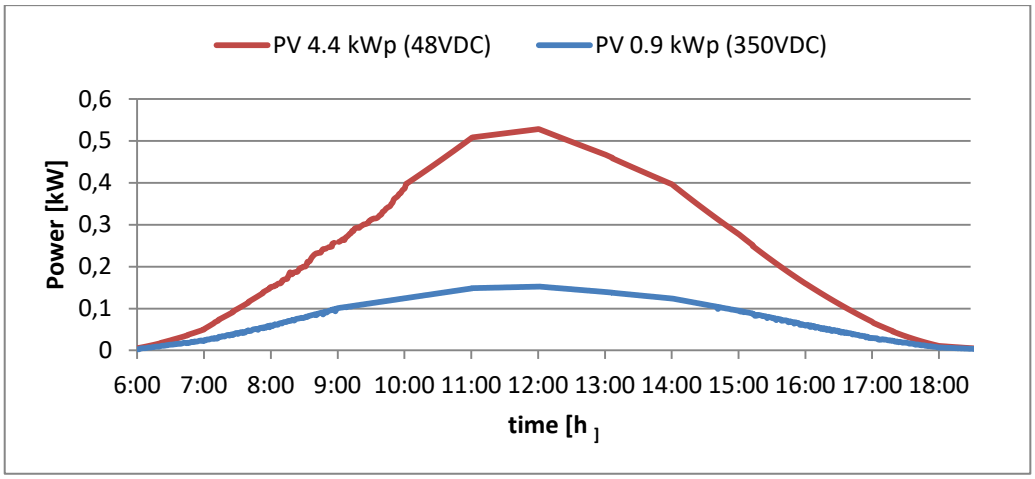

Figure 51: Daily PV panels production in September 2016 (first simulation).

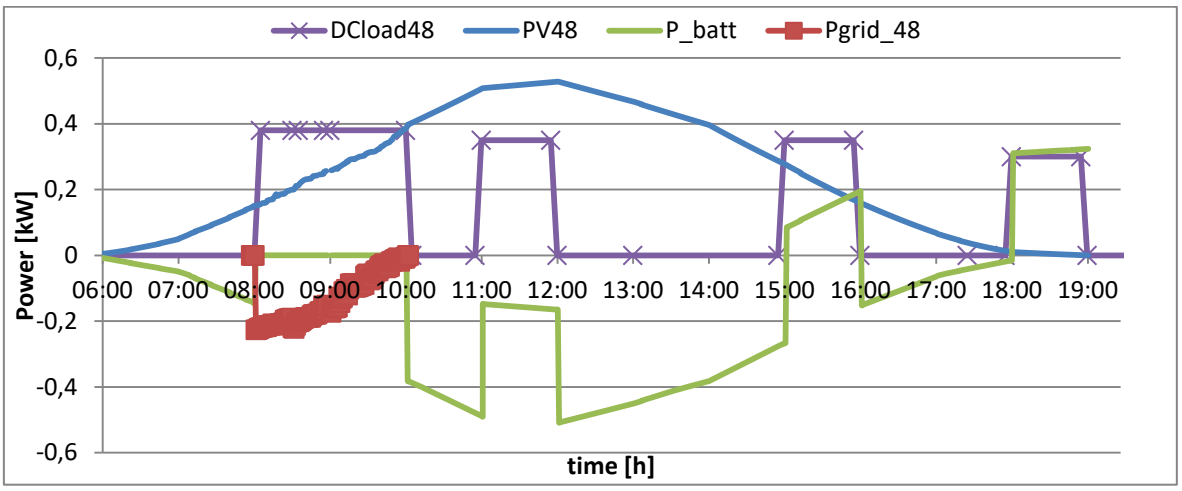

Figure 52: Daily energy balance in the low voltage line 48 V_{DC} (September, first simulation).

4.9.2. Second simulation results

In the second simulation the connection to the utility grid is not necessary yet, in contrast to the results of the first simulation of September. The charge in the batteries is still around 90% for most of the time in the month; it starts to decrease just at the end of September, see Figure 53. The charge is sometimes fixed to 90% longer time in the month and it happens because of the weekends; then during the work days the discharging scheme is nearly the same each week. It looks like a daily step function: the state of charge of the batteries is usually discharged in the evening from 90% to 86% and the day after is charged again up to 90%.

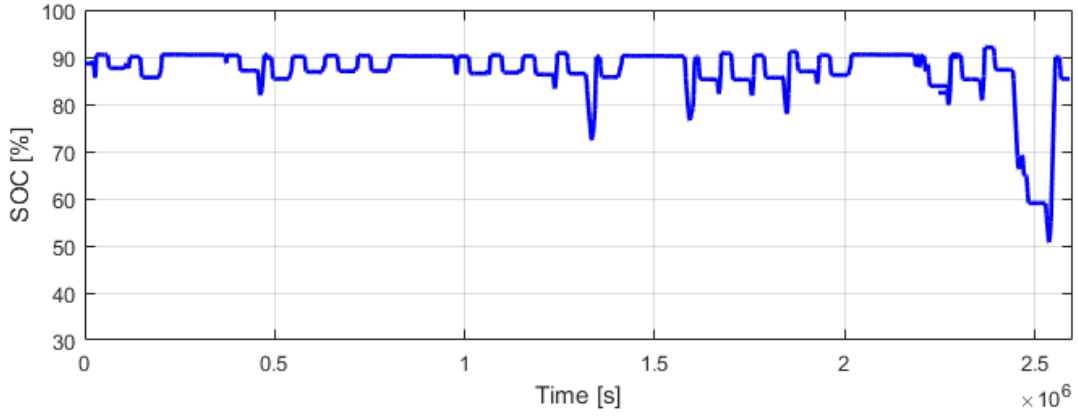

Figure 53: Battery state of charge in [%] (September, second simulation).

Figure 54 shows that in September the daily solar production is very irregular (purple line). The batteries are fully charged in a few hours in the morning (yellow line). The DC loads are always below the curve of the photovoltaic panels; that means the excess of energy is extremely variable in the studied month but it is still enough to charge loads and batteries.

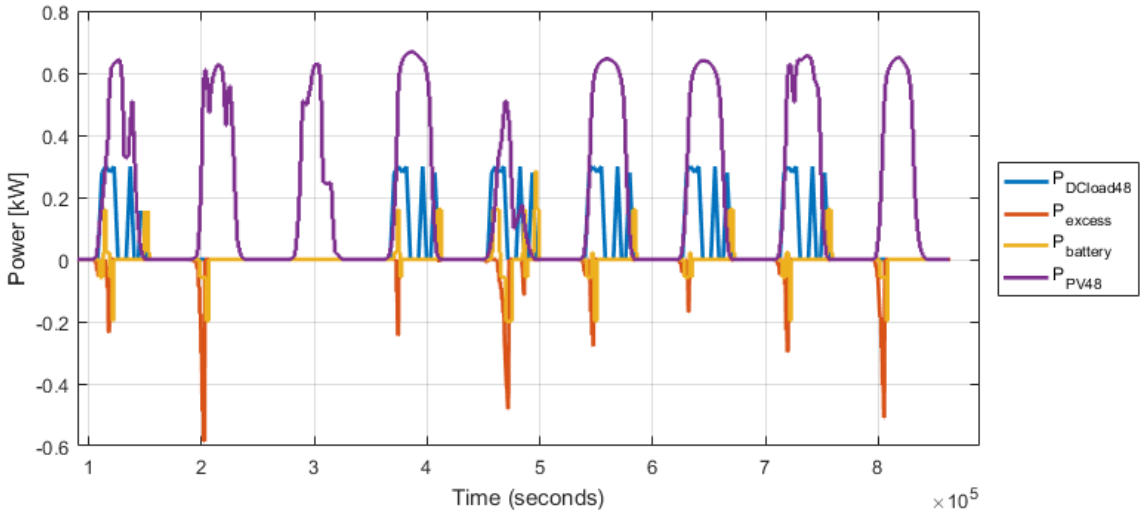

Figure 54: Energy balance in low voltage line (September 2nd – 10th , second simulation).

4.10. October 2016

The solar irradiance in October decreases a lot during the month. The maximum input is 200 W/m² just one day on October 5th, while the minimum value of 50 W/m² is reached three times.

In October, the main grid is compulsory in both voltage lines. The batteries are totally discharged for the first time during the evening on October 20th. Daytime gets shorter and the solar panels can work from 7 am to 5 pm, roughly.

4.10.1. Second simulation results

In Figure 55 and in Figure 56 it is clearly visible why the AC connection is necessary in October. The heating system is turned on also because the temperature goes below zero some days; but the solar production in the high voltage line is too low, see Figure 55.

Figure 56 shows that there are some days when the solar production (purple line) is lower than the DC loads (blue curve), thus the batteries (yellow line) supply them. Particularly, in the second half of the month, the batteries are discharged too fast and too often because of lack of solar energy production, thus AC supply is needed.

It is interesting to remark some detail between Figure 56 and Figure 57. Batteries are charged and achieve the maximum state of charge in the month thanks to the weekends when the DC loads are assumed off. During the last weekend of October (28th – 29th), batteries get just 59% because they are totally discharged the days before those.

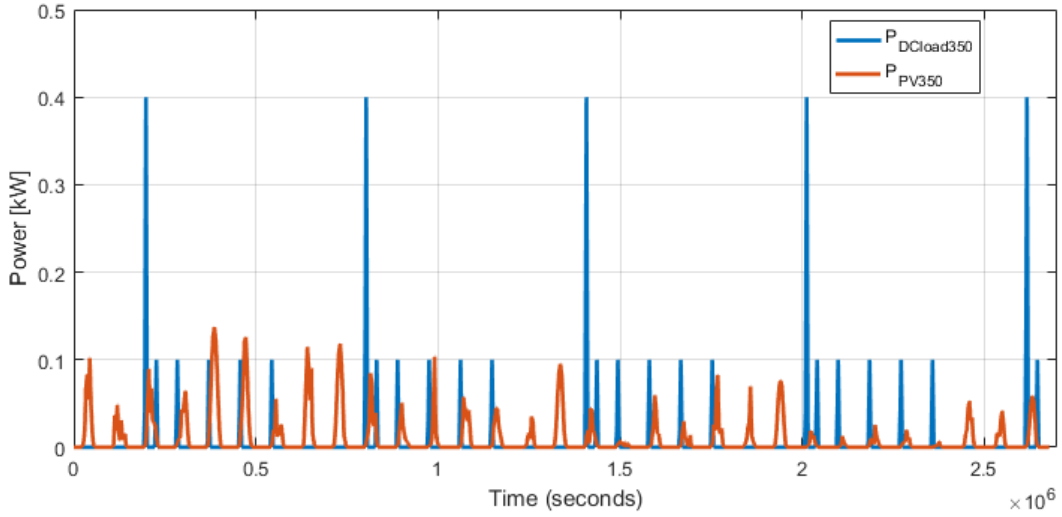

Figure 55: Monthly energy balance in the high voltage line (October, second simulation).

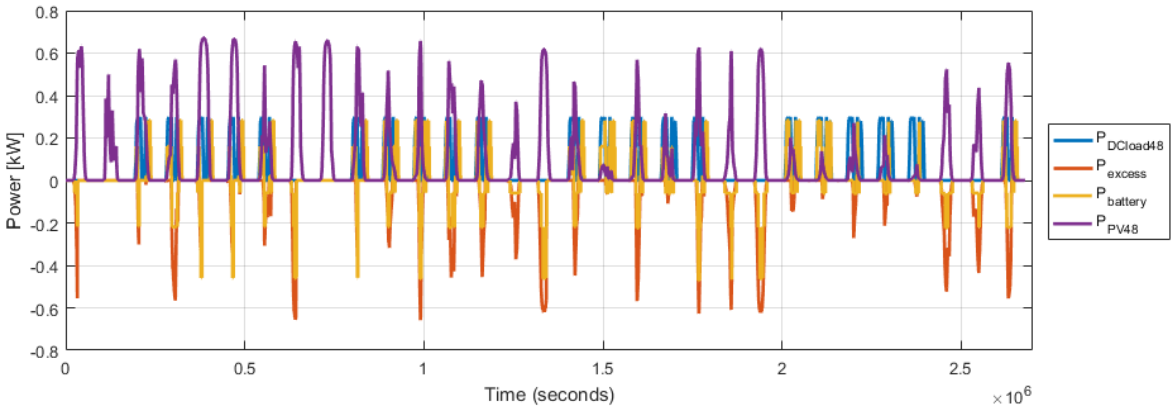

Figure 56: Monthly energy balance in the low voltage line (October, second simulation).

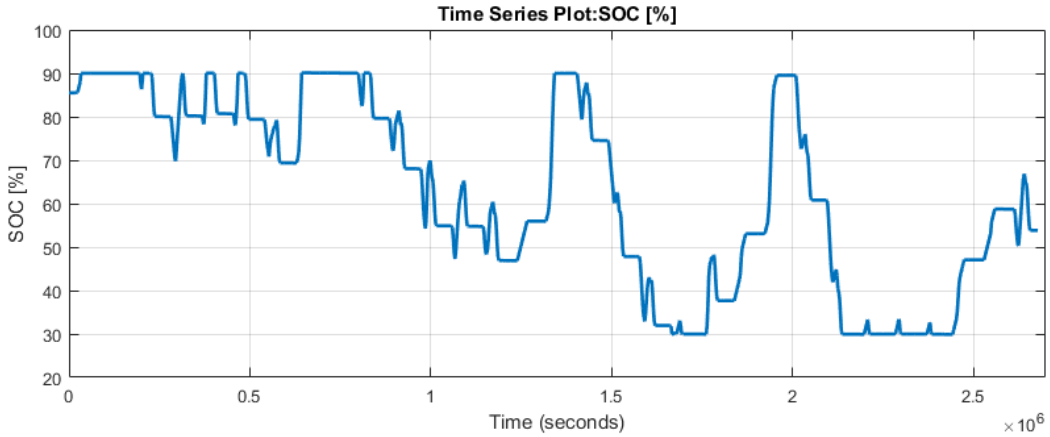

Figure 57: Battery state of charge in [%] (October, second simulation).

4.11. November 2016

The results in November are quite the same as the first months of the studied year. The solar production is nearly useless in both systems and in both simulation because of two main reasons: the irradiance is reduced and the load consumption is increased.

In the first simulation, the peak power is 0.12 kW in the bigger system and 0.05 kW in the smaller system. The batteries are charged up to 24.47% in the average day. Thus, the obvious conclusion is that the main grid is the main way to supply energy.

The second simulation makes the same point. The batteries start the run with 52% and they

are fully discharged already on November 1st. The charge is around 40% or 45% just because of weekends; then it goes again to the lowest level on the following Monday, see Figure 58.

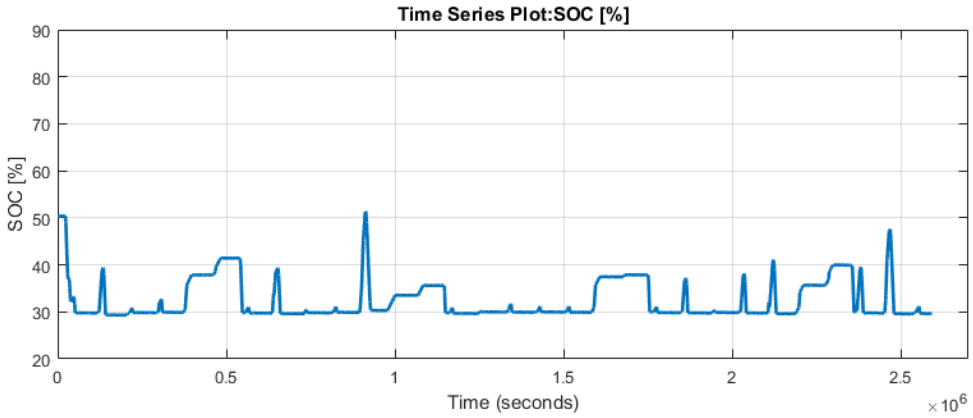

Figure 58: Battery state of charge in [%] (November, second simulation).

4.12. December 2016

The last month of the analysis presents the lowest solar irradiance values ever. December 4th is the only day with the maximum input of 100 W/m² in the month. The monthly average peak reaches barely 50 W/m². The day goes from 8 am to 4 pm. Thus, it is easy to understand that the solar systems are nearly inefficient. The charge in the batteries is kept to the lowest value every day, except on December 4th which is a Sunday. This means that the entire solar production is sent to the batteries that are able to reach 56% state of charge in that day.
The main grid is the main source of energy to the Office Lab.

5. Hydrogen production by water electrolysis

The opportunity to integrate hydrogen technology is studied thanks to the results of the second simulation. The study saves data in terms of daily values of an excess of energy during the whole year and the period when the excess occurs in [s] every day.
The values are collected in Table 4 per month. The first column describes only the months when the excess of production occurs, while the second column shows exactly how many days in the month present the availability to produce hydrogen. The last two columns give an idea about the average daily peak in excess of energy and the average daily time span. There are just three months without any hydrogen production in Table 4; there is no excess in solar production during the winter season (January, November, December).

Table 4: Monthly data collection using the yearly results of the second simulation.

	#days	average maximum daily excess [W]	average daily time span [h]
January	0	-	-
February	2	670,00	5,56
March	14	641,14	5,58
April	26	672,04	8,07
May	27	635,68	9,82
June	23	632,15	9,04
July	28	662,53	10,65
August	28	657,04	10,75
September	25	619,52	6,72
October	9	583,64	4,97
November	0	-	-
December	0	-	-

The model aims to analyse a proton exchange membrane PEM fuel cell system. The authors in (39) give the suggestion to build a theoretical model and to design the electrolyser system starting with the calculation of the amount of energy needed for electrolysis process and then the size of the water electrolyser needed to produce hydrogen.
The principle of the electrolyser is to split the water molecule into hydrogen and oxygen by giving energy (endothermic reaction).
The analysis is based on plots of the polarization curve (V-I curve) and the efficiency curve of the electrolyser, shown in Figure 59:.
The parameters of the case study are selected taking into account the values in (39); thus, the area of the PEM fuel cell is chosen 50.6 cm^2 and the electrolyser area is 100 cm^2 in order to calculate the current density. The partial pressure of the hydrogen, water and oxygen is atmospheric pressure and the operational temperature is fixed at 70°C.
Whereas it is assumed that the PEM electrolyser cell works as in Figure 59, the energy required by the electrolyser is calculated for a given efficiency. More in detail, it is assumed that the electrolyser works with 80% efficiency. This means that the electrolyser achieves 0.6 A/cm^2 when the cell voltage is 1.85 V. Thus, the cell gives the maximum power density of 1.11 W/cm^2.
Then, the number of cells in the electrolyser is calculated according to the daily excess of production available in the simulation. It is assumed that the cells are connected in series in order to increase the voltage. The first idea was to connect directly the hydrogen technology

to the low voltage line, 48 V_{DC} but the total voltage obtained is still lower than the predicted one. This means that a DC/DC buck converter is needed in the system. The second step is to calculate the hydrogen flow rate in [kg/s] using Equation (7). In order to measure the daily amount of hydrogen produced thanks to the excess of energy, the hydrogen flow rate is multiplied by the time in [s].

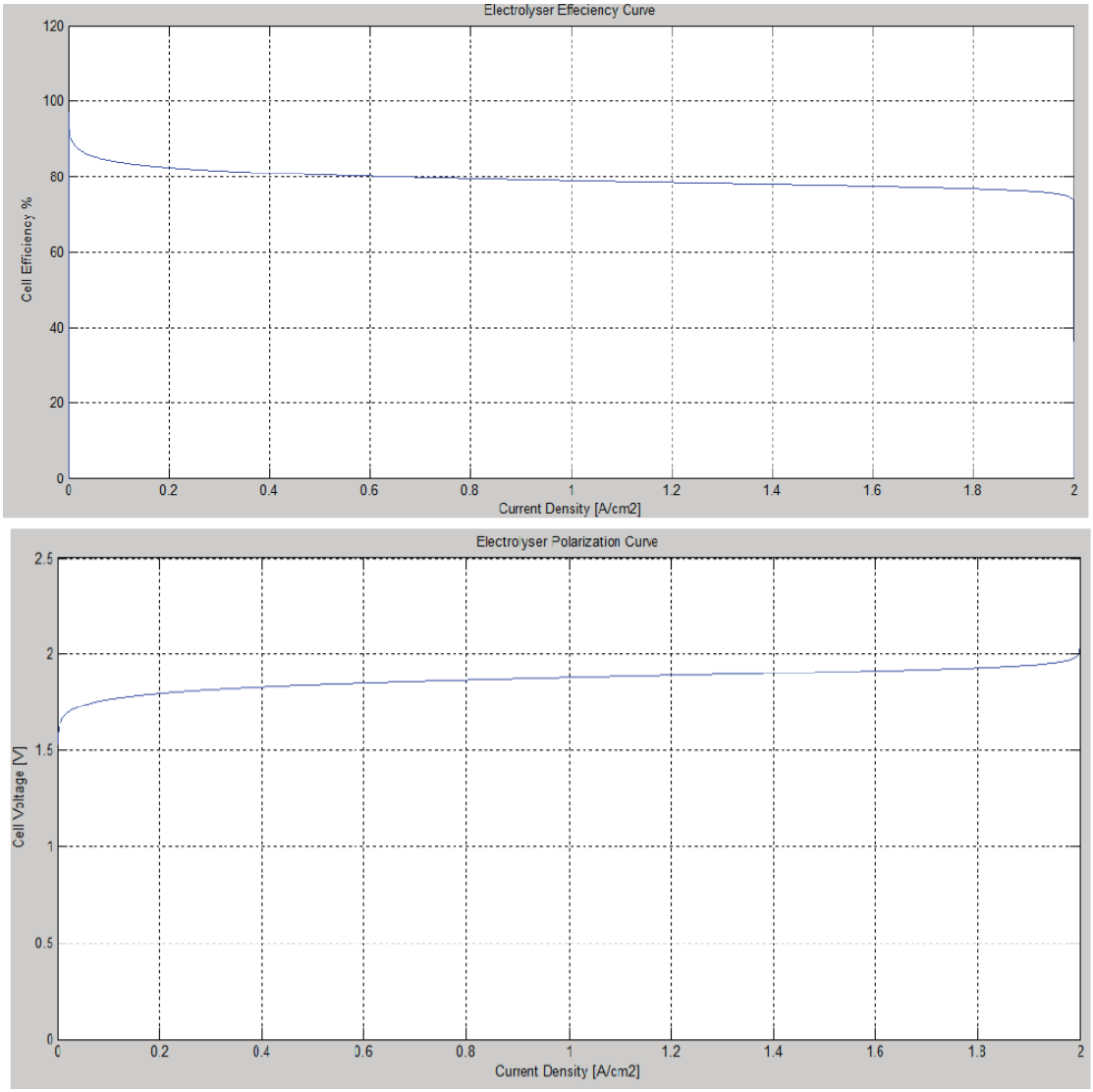

Figure 59: PEM Electrolyser Cell Polarization curve (plot above) and efficiency curve (plot below), studied in (39).

The monthly results are shown in Table 5. The first column shows the average daily production each month and the second one is the monthly result as a sum of daily productions of hydrogen.

It is important to highlight the third column in Table 5. It is the total working hours of the electrolyser. The excess of the solar production is available 18.4% of the time in one year (more precisely 1613 h over 8760 h) in the system composed by the solar system 4.4 kW_P.

In order to understand if the microgrid of The Office Lab covers the demand by hydrogen scooter, it should be remarked that two canisters of 45 g each are used in the hydrogen scooter. The main outcome is that only in summer more than one fuel cell electric vehicle is charged, from April to September exactly. The system is able to supply maximum five hydrogen scooters from no charge to full charge of hydrogen in the storages in May, July and

August, see Table 6.

Table 5: Monthly hydrogen production and total production hours.

	Average daily hydrogen production [g/day]	Monthly amount of hydrogen [kg/month]	Total monthly working hours [hour]
February	8,60	0,017	11,11
March	7,11	0,114	78,11
April	13,92	0,362	209,69
May	18,53	0,500	265,22
June	14,12	0,325	220,50
July	17,08	0,478	331,77
August	17,38	0,487	283,53
September	10,87	0,275	167,91
October	8,28	0,073	44,72
Annual	-	2,63	1612,56

Table 6: Monthly amount of fuel cell electric vehicles charged using the excess of energy in the microgrid.

	#canister		#scooter
February	0	(0,38)	0
March	2	(2,53)	1
April	8	(8,04)	4
May	11	(11,12)	5,5
June	7	(7,22)	3,5
July	10	(10,62)	5
August	10	(10,81)	5
September	6	(6,11)	3
October	1	(1,63)	0,5
Annual	58		29

The results commented above are based on the assumption of using each day the best configuration in terms of operating voltage, efficiency and, consequently, in terms of the number of cells in the electrolyser. Thus, each day the electrolyser works using almost entirely the excess of energy and its size changes daily in the idea of the best operating condition. From a technological point of view, a real system could work only with a fixed size of the system during the year. Therefore, the design of the hydrogen technology is studied according to the collected data. The system has to work with the best efficiency as long as possible. The electrolyser is composed by five cells for most of the time in the year. Thus, five cells connected in series are chosen, which should operate with voltage 9.25 V_{DC}. As a result, the size of the PEM electrolyser, that should be installed in the microgrid, is 555 W. In this way, those days with lower excess in solar production work with even lower efficiency; while those with bigger excess are clearly limited in terms of hydrogen production. In the end, the final results are worse than the previous case (Table 5 and Table 6) studied with the best daily configuration. Table 7 shows the comparison between the two design configurations described above in terms of monthly and yearly hydrogen production. An important outcome is that the annual production is reduced just by 500 g. This means that the system is working close to the best performance.

Table 7: Comparison between the best daily design and the fixed size of electrolyser.

	Monthly amount of hydrogen BEST DAILY CONFIGURATION [kg/month]	Monthly amount of hydrogen 5CELLs [kg/month]
February	0,017	0,012
March	0,114	0,090
April	0,362	0,254
May	0,500	0,384
June	0,325	0,295
July	0,478	0,379
August	0,487	0,410
September	0,275	0,206
October	0,073	0,052
annual	2,63	2,08

6. Conclusion

The aim of this paper was the evaluation of the technical performances of a microgrid composed of the office, PV panels, batteries, loads and connection to the AC grid. After the collection of the annual results of both simulation (see Chapter 4), it is important to highlight some details and comments. During the winter season, from January to March and from October to December, the main grid is essentially required in the Office Lab to feed the loads. Indeed, in winter the combination of low solar irradiance and high load consumptions implies that the batteries are discharged until their minimum state of charge. Anyway, it is worth to say that during the weekend the DC loads are assumed off in the two meeting rooms; thus if the weather conditions are good, the batteries can at least be charged above the minimum value in those months. This is the reason why in February for the first time in the year the batteries are able to reach the maximum state of charge on February 17th. Hence, the excess in solar production occurs for the first time in the year for 11 hours and the amount of nearly 20 g of hydrogen are produced.

Starting from March to October, the monthly solar irradiance is nearly every day above the load profiles, except some cloudy days. The main outcome is that batteries are charged during the day; therefore, they can supply the microgrid of the office when the sun goes down during the evening and in the early morning of the day after, if the charge is enough. The associated result is that from March to October hydrogen is always available with a total amount of 2.614 kg, which is nearly equal to the yearly production. Indeed, the paper has calculated also the excess of energy when the batteries are fully charged, which permitted to produce the annual amount of hydrogen equal to 2.63 kg in nine months, from February to October.

Conversely, the part of the microgrid tested in the high voltage line is quite inefficient because of the load profile. The heating system is the only DC load associated to that part of the microgrid, but the solar area installed is inadequate compared to the consumption in the IR panels. Therefore, more panels should be connected to the 350 V_{DC} or the PV systems in the two voltage lines should interact in order to supply the Office Lab in the smartest and the most efficient way possible.

The study was integrated into the CaPP project in terms of the amount of hydrogen produced by the excess of energy. The storage units are chosen as canisters of the Fuel Cell lightweight Electric Vehicles.

The main aim of this work was the possibility to avoid the energy sent to the main grid and to use the yearly excess of solar production for nine months.

The combination of solar systems and batteries made possible the increase in the self-consumption of solar energy and the reduction of the daily energy dependence from the grid. A further positive aspect of the analysis is that the loads consumption in the office is nearly in phase with daily solar production. The consumption and production profiles in the resolution of minute data allowed an efficient matching of the request and utilization of the generation resources.

On the other hand, the main problem was that the microgrid needed necessarily the AC grid to supply loads during the winter season and cloudy days in a row. If the Office Lab should work in stand-alone mode, other distributed energy resources ought to be considered. Indeed, the total results of this case study cannot be enhanced only by increasing the PV panels area or increasing the size of batteries because the main issue is the lack of a big amount of solar radiation in The Netherlands, particularly during winter. Thus, other on-site generation sources could include the implementation of small wind turbines or fuel cell vehicles and/or electric vehicles in vehicle-to-load connection to supply the office loads.

It is important to highlight that the results obtained in this work are strongly influenced by the solar irradiance levels. As an example, in the North of Italy, the same system could work completely in standalone mode. Clearly, if the location of the measurement changes and if the irradiance increases, other parameters should be also calculated accurately because they can affect the performance of the system, like the temperature influence and also the possibility of mismatch due to shading effects in the operating condition of the solar system.

6. 1. Future developments

The combination of solar and wind resources in different parts of the world could be studied in future research.

According to the analysis performed in these pages, the integration of renewable energy sources needs storage solutions to support the energy demand in buildings like offices or houses. Particularly, seasonal energy storages should be implemented because the main issue was to fulfill the loads during the winter season, in line with the yearly results obtained.

Indeed, the hydrogen scooters could work in discharge mode to supply the loads as well as batteries. In this case, more variables should be considered like as the minimum number of scooters needed, the availability of the vehicles during a day and the unpredictable state of charge of the canisters in the morning. This future study could include also the surplus of heat generated in the fuel cell; it can be used to reduce the consumption of the heating system.

On the other hand, real measurements about the loads are helpful to evaluate more exactly the hydrogen production. Simultaneously, real-time information about the energy balances could permit to monitor and to regulate the habits of the occupants towards lowering the consumption from the main grid and, consequently, costs. Clearly, real-life variations could be expected due to different occupation rates and different living styles of the occupants.

Another important parameter is the feasibility of the system from an economic point of view, in terms of costs of installation and the possibility of recharging the hydrogen vehicles using the main grid when it is more convenient. Nowadays, hydrogen fuel cell based devices could be used for transport and power generation purposes but they are overcome by cheaper and less efficient power plant in electricity production. In the near future, a revolution in the energy and transport sector is mandatory for the transition toward a world based on 100% exploitation of renewable energy sources. Thus, the estimation of annual expenses could be the subject for future developments of the project to identify the best configuration in order to integrate hydrogen devices.

One more crucial topic is the legislation. Despite several model limitations, the results in these pages show the advantages of the combination of transport and residential sectors in a more sustainable energy system. Energy policies should be acquired in order to promote consumer information and awareness. The configuration of the system presented in these pages could become an interesting option for end-users to reduce their electricity bills and to use the on-site production in the smartest way possible.

7. References

1. **European Environmental Agency.** Final energy consumption by sector. [Online] 2016. https://www.eea.europa.eu/data-and-maps/daviz/total-final-energy-consumption-by-sector-2#tab-chart_3.

2. **European Commission .** 2050 low-carbon economy. *Energy, Climate change, Environment - Climate action.* [Online] https://ec.europa.eu/clima/policies/strategies/2050_en.

3. **International Energy Agency.** Technology Roadmap - Smart grids. 2011, p. 52. https://www.iea.org/publications/freepublications/publication/technology-roadmap-smart-grids.html.

4. **The Green Village.** [Online] https://www.thegreenvillage.org/.

5. **Oxford Dictionaries.** [Online] https://www.oxforddictionaries.com/.

6. **Geert P.J. Verbong, Sjouke Beemsterboer, Frans Sengers.** Smart grids or smart users? Involving users in developing a low carbon electricity economy. *Energy Policy, Volume 52.* 2013, p. 117-125. https://doi.org/10.1016/j.enpol.2012.05.003..

7. **Willett Kempton, Jasna Tomić.** Vehicle-to-grid power implementation: From stabilizing the grid to supporting large-scale renewable energy. *Journal of Power Sources.* 2005, Vol. 144, 1, p. 280-294. https://doi.org/10.1016/j.jpowsour.2004.12.022..

8. **Electric power research institute.** *Electricity Technology Roadmap: Meeting the Critical Challenges of the 21st Century : 2003 Summary and Synthesis.* s.l. : Electric Power Research Institute (EPRI), 2003. p. 4-8. https://books.google.nl/books?id=aKeDNwAACAAJ. Product number 1010929.

9. **European Photovoltaic Industry Association.** Self consumption of PV electricity. *Renewable Energy House.* 2013, p. 17.

10. **Henrik Lund, Willett Kempton.** Integration of renewable energy into the transport and electricity sectors through V2G. *Energy Policy.* 2008, Vol. 36, 9, p. 3578-3587. https://doi.org/10.1016/j.enpol.2008.06.007..

11. **S.-L. Andersson, A.K. Elofsson, M.D. Galus, L. Göransson, S. Karlsson, F. Johnsson, G. Andersson.** Plug-in hybrid electric vehicles as regulating power providers: Case studies of Sweden and Germany. *Energy Policy.* 2010, Vol. 38, 6, p. 2751-2762. https://doi.org/10.1016/j.enpol.2010.01.006..

12. **Robert Hein, Paul R. Kleindorfer, Stefan Spinler.** Valuation of electric vehicle batteries in vehicle-to-grid and battery-to-grid systems. *Technological Forecasting and Social Change.* 2012, Vol. 79, 9, p. 1654-1671. https://doi.org/10.1016/j.techfore.2012.06.002..

13. **Tiago Sousa, Hugo Morais, João Soares, Zita Vale.** Day-ahead resource scheduling in smart grids considering Vehicle-to-Grid and network constraints. *Applied Energy.* 2012, Vol. 96, p. 183-193. https://doi.org/10.1016/j.apenergy.2012.01.053..

14. **Mart van der Kam, Wilfried van Sark.** Smart charging of electric vehicles with photovoltaic power and vehicle-to-grid technology in a microgrid; a case study. *Applied Energy.* 2015, Vol. 152, p. 20-30. http://www.sciencedirect.com/science/article/pii/S0306261915005553.

15. **Petra Mesarić, Slavko Krajcar.** Home demand side management integrated with electric vehicles and renewable energy sources. *Energy and Buildings.* 2015, Vol. 108, p. 1-9. http://www.sciencedirect.com/science/article/pii/S0378778815302425.

16. **Kari Alanne, Sunliang Cao.** Zero-energy hydrogen economy (ZEH2E) for buildings and communities including personal mobility. *Renewable and Sustainable Energy Reviews.* 2017, Vol. 71, p. 697-711. http://www.sciencedirect.com/science/article/pii/S1364032116311546.

17. **Xiongwen Zhang, Siew Hwa Chan, Hiang Kwee Ho, Siew-Chong Tan, Mengyu Li, Guojun Li, Jun Li, Zhenping Feng.** Towards a smart energy network: The roles of fuel/electrolysis cells and technological perspectives. *International Journal of Hydrogen Energy.* 2015, Vol. 40, p. 6866-6919. http://www.sciencedirect.com/science/article/pii/S036031991500779X.

18. **A. Yunez-Cano, R. de G. González-Huerta, M. Tufiño-Velázquez, R. Barbosa, B. Escobar.** Solar-hydrogen hybrid system integrated to a sustainable house in Mexico. *International Journal of Hydrogen Energy.* 2016, Vol. 41, p. 19539-19545. http://www.sciencedirect.com/science/article/pii/S036031991630307X.

19. **Sunliang Cao, Konstantin Klein, Sebastian Herkel, Kai Sirén.** Approaches to enhance the energy performance of a zero-energy building integrated with a commercial-scale hydrogen fueled zero-energy vehicle under Finnish and German conditions. *Energy Conversion and Management.* 2017, Vol. 142, p. 153-175. http://www.sciencedirect.com/science/article/pii/S0196890417302510.

20. **Miri Motalleb, Ankica Đukić, Mihajlo Firak.** Solar hydrogen power system for isolated passive house. *International Journal of Hydrogen Energy.* 2015, Vol. 40, p. 16001-16009. http://www.sciencedirect.com/science/article/pii/S0360319915303050.

21. **Farid Alavi, Esther Park Lee, Nathan van de Wouw, Bart De Schutter, Zofia Lukszo.** Fuel cell cars in a microgrid for synergies between hydrogen and electricity networks. *Applied Energy.* 2017, Vol. 192, p. 296-304. http://www.sciencedirect.com/science/article/pii/S0306261916315288.

22. **Cao, Sunliang & Alanne, Kari.** Technical feasibility of a hybrid on-site H2 and renewable energy system for a

zero-energy building with a H2 vehicle. *Applied Energy.* 2015, Vol. 158, 1, p. 568-583. https://www.researchgate.net/publication/281774266_Technical_feasibility_of_a_hybrid_on-site_H_2_and_renewable_energy_system_for_a_zero-energy_building_with_a_H_2_vehicle.
23. **Guille, Christophe e Gross, George.** A conceptual framework for the vehicle-to-grid (V2G) implementation. *Energy Policy.* 2009, Vol. 37, 11, p. 4379-4390. https://doi.org/10.1016/j.enpol.2009.05.053.
24. **Ad van Wijk, Leendert Verhoef.** *Our car as power plant.* Delft : IOS Press BV, 2014. ISBN 978-1-61499-377-3.
25. **B. Wunder, L. Ott, M. Szpek, U. Boeke, R. Weiß.** Energy efficient DC-grids for commercial buildings. *2014 IEEE 36th International Telecommunications Energy Conference (INTELEC).* 2014, p. 1-8. http://ieeexplore.ieee.org/stamp/stamp.jsp?tp=&arnumber=6972215&isnumber=6972109.
26. *DC Power Grids for buildings.* **U. Boeke, M. Wendt.** 2015, IEEE First International Conference on DC Microgrids (ICDCM), p. 210-214.
27. *Direct Current in public lighting for improvement in LED performance and costs.* **M. Hulsebosch, P. Willigenburg, J. Woudstra, B. Groenewald.** 2014. International Conference on the Eleventh industrial and Commercial Use of Energy. p. 1-9.
28. **Joint Research Centre. Institute for Energy and Transport.** Photovoltaic Geographical Information System (PVGIS). [Online] http://re.jrc.ec.europa.eu/pvgis/.
29. **Koninklijk Nederlands Meteorologisch Instituut (KNMI).** Royal Metherlands Meteorological Institute. [Online] https://www.knmi.nl/over-het-knmi/about.
30. **Arpa Lombardia. Agenzia Regionale per la protezione dell'ambiente ambientale in Lombardia.** [Online] http://www.arpalombardia.it/Pages/ARPA_Home_Page.aspx.
31. **R. Weiss, L. Ott and U. Boeke.** Energy efficient low-voltage DC-grids for commercial buildings. *2015 IEEE First International Conference on DC Microgrids (ICDCM).* 2015, p. 154-158. http://ieeexplore.ieee.org/stamp/stamp.jsp?tp=&arnumber=7152030&isnumber=7151990.
32. **Climatic Klimaatbeheersing.** [Online] http://www.climatic.nl/.
33. **Wikipedia, the Free Encyclopedia.** Passive Sign convention. [Online] https://en.wikipedia.org/wiki/Passive_sign_convention.
34. *Simulation and Designing of MPPT based solar PV ststem with DC-DC Boost converter.* **Dayaramani R., Bharadwaj S. K., Gawre S.** 7, s.l. : Internation Journal of Engineering Technology Science and Research IJETSR, 2017, Vol. 4. https://www.researchgate.net/publication/320258427_Simulation_and_Designing_of_MPPT_Based_Solar_PV_System_with_DC-DC_Boost_Converter. ISSN 2394-3386.
35. **F. Vasca, L. Iannelli.** *Dynamics and Control of Switched Electronic Systems: Advanced Perspectives for Modeling, Simulation and Control of Power Converters.* 1447128850. s.l. : Springer Science & Business Media, 2012. p. 494. https://books.google.nl/books?id=J8GIj68VnSUC.
36. **MathWorks.** [Online] https://it.mathworks.com/.
37. **U.S. Department of Energy, Office of Energy Efficiency and Renewable energy.** *2013 Fuel Cell Technologies Market Report.* 2013. p. 37. https://energy.gov/sites/prod/files/2014/11/f19/fcto_2013_market_report.pdf.
38. **Asia Pacific Fuel Cell Technologies (APFCT) Ltd.** [Online] http://www.apfct.com/en/.
39. **Eng. Waseem Saeed, Eng. Ghaith Warkozek.** Modeling and Analysis of Renewable PEM Fuel Cell System. *Energy Procedia.* 2015, Vol. 74, p. 87-101. http://www.sciencedirect.com/science/article/pii/S1876610215012953.
40. **R. Kemp, J.W. Schot, R. Hoogma.** Regime shifts to sustainability through processes of niche formation: the approach of strategic niche management. *Technology Analysis and Strategic Management.* 1998, Vol. Vol. 10 , No. 2, p. 175-195 . https://pure.tue.nl/ws/files/3276894/Metis238779.pdf.
41. *Technology Roadmap: Smart Grid.* **International Energy Agency.** 2011, p. 52.
42. **Raven, Rob.** Niche accumulation and hybridisation strategies in transition processes towards a sustainable energy system: An assessment of differences and pitfalls. *Energy Policy.* 2007, Vol. 35, 4, p. 2390-2400. https://doi.org/10.1016/j.enpol.2006.09.003..
43. **J.W. Schot, F.W. Geels.** Strategic niche management and sustainable innovation journeys : theory, findings, research agenda, and policy. *TEchnology Analysis and Strategic Management.* 2008, Vol. 20, 5, p. 537-554. https://pure.tue.nl/ws/files/3156995/Metis218948.pdf.
44. **G. A. Laudani, P. D. Mitcheson.** Comparison of cost and efficiency of DC versus AC in office buildings. *Transformation of the Top and Tail of Energy Networks.* 2015, p. 1-52.
45. **Delft University of Technology.** *The scooter as mini Power Plant.* Delft : s.n., 2017. https://www.tudelft.nl/en/2017/3me/the-scooter-as-mini-power-plant/.